remote sensing

MDPI

Article

Assessing the Potential of Backpack-Mounted Mobile Laser Scanning Systems for Tree Phenotyping

Robin J. L. Hartley [1,*], Sadeepa Jayathunga [1], Peter D. Massam [1], Dilshan De Silva [1], Honey Jane Estarija [1], Sam J. Davidson [2], Adedamola Wuraola [2,3] and Grant D. Pearse [1]

[1] Scion, 49 Sala Street, Private Bag 3020, Rotorua 3046, New Zealand; sadeepa.jayathunga@scionresearch.com (S.J.); peter.massam@scionresearch.com (P.D.M.); dilshan.desilva@scionresearch.com (D.D.S.); honey.estarija@scionresearch.com (H.J.E.); grant.pearse@scionresearch.com (G.D.P.)

[2] Scion, 10 Kyle Street, Riccarton, Christchurch 8011, New Zealand; sam.davidson@scionresearch.com (S.J.D.); adedamola.wuraola@imagr.co (A.W.)

[3] Imagr Ltd., 16 Maidstone Street, Grey Lynn, Auckland 1021, New Zealand

* Correspondence: robin.hartley@scionresearch.com

Abstract: Phenotyping has been a reality for aiding the selection of optimal crops for specific environments for decades in various horticultural industries. However, until recently, phenotyping was less accessible to tree breeders due to the size of the crop, the length of the rotation and the difficulty in acquiring detailed measurements. With the advent of affordable and non-destructive technologies, such as mobile laser scanners (MLS), phenotyping of mature forests is now becoming practical. Despite the potential of MLS technology, few studies included detailed assessments of its accuracy in mature plantations. In this study, we assessed a novel, high-density MLS operated below canopy for its ability to derive phenotypic measurements from mature *Pinus radiata*. MLS data were co-registered with above-canopy UAV laser scanner (ULS) data and imported to a pipeline that segments individual trees from the point cloud before extracting tree-level metrics. The metrics studied include tree height, diameter at breast height (DBH), stem volume and whorl characteristics. MLS-derived tree metrics were compared to field measurements and metrics derived from ULS alone. Our pipeline was able to segment individual trees with a success rate of 90.3%. We also observed strong agreement between field measurements and MLS-derived DBH (R^2 = 0.99, RMSE = 5.4%) and stem volume (R^2 = 0.99, RMSE = 10.16%). Additionally, we proposed a new variable height method for deriving DBH to avoid swelling, with an overall accuracy of 52% for identifying the correct method for where to take the diameter measurement. A key finding of this study was that MLS data acquired from below the canopy was able to derive canopy heights with a level of accuracy comparable to a high-end ULS scanner (R^2 = 0.94, RMSE = 3.02%), negating the need for capturing above-canopy data to obtain accurate canopy height models. Overall, the findings of this study demonstrate that even in mature forests, MLS technology holds strong potential for advancing forest phenotyping and tree measurement.

Keywords: lidar; MLS; SLAM; UAV; ULS; tree form; mensuration

Citation: Hartley, R.J.L.; Jayathunga, S.; Massam, P.D.; De Silva, D.; Estarija, H.J.; Davidson, S.J.; Wuraola, A.; Pearse, G.D. Assessing the Potential of Backpack-Mounted Mobile Laser Scanning Systems for Tree Phenotyping. *Remote Sens.* **2022**, *14*, 3344. https://doi.org/10.3390/rs14143344

Academic Editors: Markus Eichhorn and Ting Yun

Received: 10 June 2022
Accepted: 8 July 2022
Published: 11 July 2022

1. Introduction

Digital phenotyping is an emerging science that uses non-invasive techniques, such as laser scanning, to assess the interaction between genetics, environmental factors and silviculture (GxExS) to guide the selection of the most productive trees for a given environment [1]. In forestry, phenotyping is emerging as a means of selecting the right tree, for the right place, for the right purpose, and to increase the efficiency of tree breeding programmes [2]. Current phenotyping methodologies require the combination of GxExS data with the physical description of tree form [3]. Traditional methods for the physical

description of tree form are manual, time-consuming, costly and error-prone—severely limiting the potential throughput [2,4].

Remote sensing (RS), on the other hand, could provide a set of convenient tools for in situ tree phenotyping, with data from sources that include airborne laser scanning (ALS) being useful for deriving information from the canopy and the terrain [3]. ALS was researched extensively for extracting tree height, stand density and crown metrics [3,5–8]. However, it is limited in its ability to describe stem form due to the heavy occlusion and limited pulse penetration caused by the dense forest canopy. The lower pulse density observed under the canopy often provides sparse three-dimensional (3D) characterisation of the stems—making it unsuitable for comprehensive tree form assessment [9]. An alternative RS data source is unmanned aerial vehicle (UAV) laser scanning (ULS) which enables close-range aerial captures over forested areas with higher pulse densities. ULS systems vary in their accuracy depending on the scanner utilised, with high-end options (e.g., Riegl VUX range) being more accurate compared with more affordable options that utilise re-purposed automotive laser scanners (e.g., Velodyne Puck range) [10]. Despite offering much higher pulse density than ALS, ULS still suffers from occlusion caused by the dense canopy.

To limit canopy occlusion, the description of tree form has often focused on RS methods, such as terrestrial laser scanning (TLS), that capture data from below the canopy. Statically-mounted TLS was explored for forestry applications for nearly two decades [11–14]. In this approach, multiple scans are acquired and aligned from different viewpoints to minimise occlusion and achieve plot-level coverage. Most recent research on statically-mounted TLS focused on topics, such as scanning forestry plots, deriving tree form metrics and assessing the efficacy of TLS as a tool for carrying out forest inventory [15–20]. Although these studies reported higher accuracy in the tree-form assessment [18], the technology was not seen as widely operational due to its impractical nature [19]. TLS also produces fewer returns from the upper stem due to occlusion from branching [21] which, in turn, reduces the accuracy in height measurement [22].

Mobile laser scanning (MLS) was introduced as an alternative to TLS and was used in forest environments since 2013 [23]. MLS systems are similar to ALS, in that they combine a laser scanner with an inertial measurement unit (IMU) and a global-navigation-satellite system (GNSS) receiver on a moving platform [24]. Arguably, it was not until the GNSS component was replaced with simultaneous localisation and mapping (SLAM) algorithms that these systems became truly suited to the forest environment where below-canopy GNSS reception is often poor. SLAM algorithms are GNSS-independent and enable the creation of locally consistent point clouds in GNSS-denied environments, such as beneath a dense forest canopy. Lightweight MLS systems are often referred to as personal, handheld or backpack laser scanners depending on the configuration of the unit. In recent years, there is a growing body of research focused on MLS application within forestry [22–26]. By their nature, MLS systems can achieve greater coverage of a forest environment in a shorter timeframe with reduced occlusion, addressing the key issues that make TLS impractical for forest inventory [27]. However, MLS systems are often restricted to integrating lightweight scanners that have large beam divergence and lower power. This limits their range and accuracy, specifically when characterising the upper part of tree stems [28,29].

Algorithms for tree-form description from lidar point clouds were developed for tree stem segmentation [30] and extraction of a wide range of metrics, including diameter at breast height (DBH) [31], stem straightness [17], stem volume [32] and branch characterisation [33]. The majority of these algorithms work on heuristic principles. Stem characterisation methods for TLS data were effectively adapted to ULS data [26,34,35], allowing for scalable measurement of tree-form metrics. However, owing to the denser canopy, a previous study that used ULS data in a mature stand of *Pinus radiata* failed to obtain a sufficient number of stem points to derive any metrics other than height [36]. This highlights the need for an efficient remote-sensing tool that can be used to improve the 3D tree characterisation below the dense forest canopy of plantation species. The efficiency gains of using MLS compared with traditional inventory methods was already

demonstrated for several popular plantation species [25] with nothing to report on *P. radiata*. Therefore, this study will pursue the potential accuracies of tree form measurement from MLS platforms under dense *P. radiata*, which is one of the most widely planted exotic pine species globally and the dominant species in the Southern Hemisphere [37,38].

Of the various metrics derived from MLS and TLS data, DBH and height received some of the widest attention in the literature and a comprehensive list of studies can be found in [18,39]. Although existing studies reported a strong correlation between point cloud-derived DBH and field-measured DBH, Bauwens et al. [24] noted that the calculation of DBH at a fixed height above the derived digital terrain model (DTM) (the fixed-height method) could potentially introduce errors. Inclusion of swelling within estimations for DBH is currently not taken into account in the existing DBH algorithms; however, this contradicts field measurement guidelines, affects the accuracy of point cloud-derived DBH and introduces errors, such as stem volume or taper, into other calculations, such as stem volume or taper. Another common finding in the literature is the inability of TLS data to accurately describe the full tree height [39]. This can be addressed through the combination of the above-canopy ULS data with the below-canopy TLS data; however, this adds additional complications and resource requirements to the operation.

DBH and height are, arguably, two of the most important tree-form metrics for foresters and tree breeders [21]. Thus, to replace traditional field measurement, any new system that is developed for phenotyping or inventory would need to address the issues with the DBH and height estimations from RS platforms. To address the issues related to the DBH height, in this study, we proposed a variable breast height (VBH) detection method that intuitively decides DBH height based on a stem-diameter profile and compared this to the fixed-height method and a method involving taking DBH measurements at the same height as field measurements (field-height method), as per [24]. We also tested the potential of MLS data to accurately describe the full tree height under a dense canopy.

While methods exist to assess metrics associated with growth and basic stem characteristics, one of the largest drivers for timber value is knottiness [40]; branching characteristics are, therefore, one of the most important phenotypic traits for foresters and breeders. Metrics, such as branch size and angle, branch frequency and branch dispersion (length of internodes) are key determinants of timber grades and, therefore, genotype value [41]. Consequently, the ability to accurately and objectively characterise branching patterns at scale is a valuable tool for phenotyping. A small body of research developed around the extraction of branching characteristics from lidar point clouds [15,33,42–44], with only a few papers focusing on the detection of branch knots or branch whorls [45–47]. However, nothing specific was developed for *P. radiata*, which is known to have more branches than most of the other needle-leaf plantation species. In this study, we developed and tested a diameter profile-based whorl detection method.

The overall aim of the study is to assess a novel, high-density MLS for its ability to segment individual trees and derive tree-form metrics, e.g., DBH, tree height and whorl height, in a mature stand of *P. radiata*. In this paper, we (1) present the results of tree-form metrics derived from MLS data utilising various algorithms; (2) compare the MLS-derived metrics with traditional field measurements and ULS-derived metrics; and (3) discuss the applicability of MLS systems in the context of tree phenotyping and commercial forestry.

2. Materials and Methods

2.1. Data Capture

2.1.1. Study Site

The Scion nursery in Rotorua, on the North Island of Aotearoa New Zealand (NZ), (Figure 1) was selected for the study site for this genetics trial. The trial stand is approximately two hectares in size and comprises *P. radiata* D. Don with an age range of eighteen to twenty years. Details of the tree size are summarised in Table 1 and Figure 2.

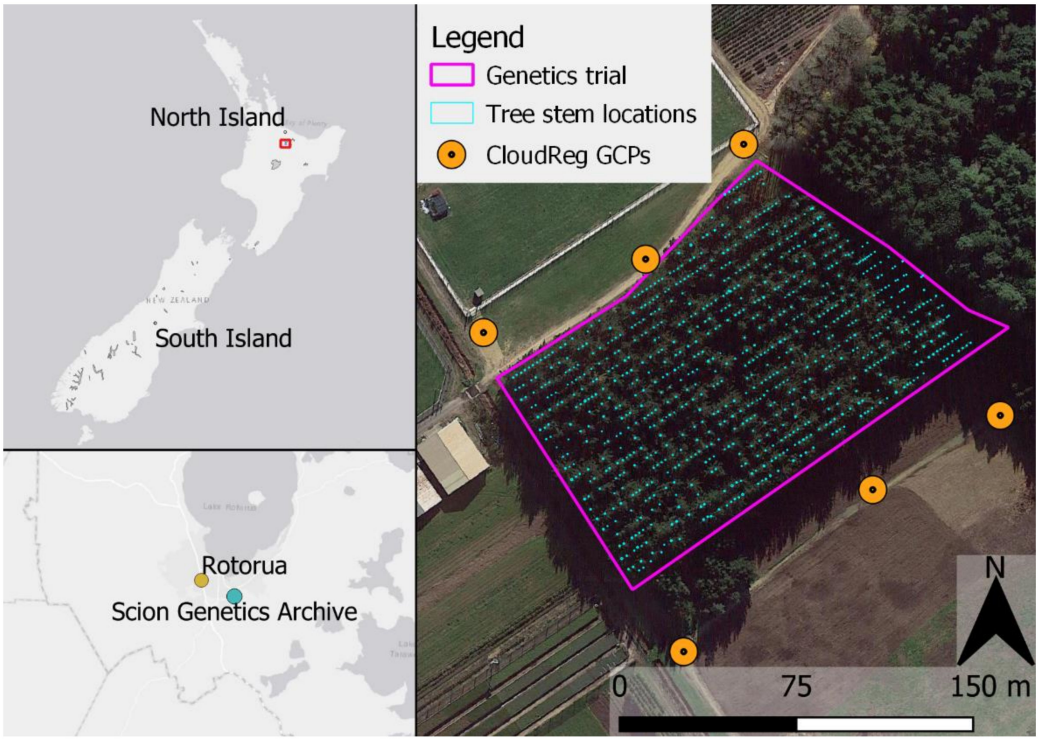

Figure 1. Map of the study site showing the area of the trial stand (purple box) and the locations of tree stems in the study (blue rings). Insets show the location of the trial site.

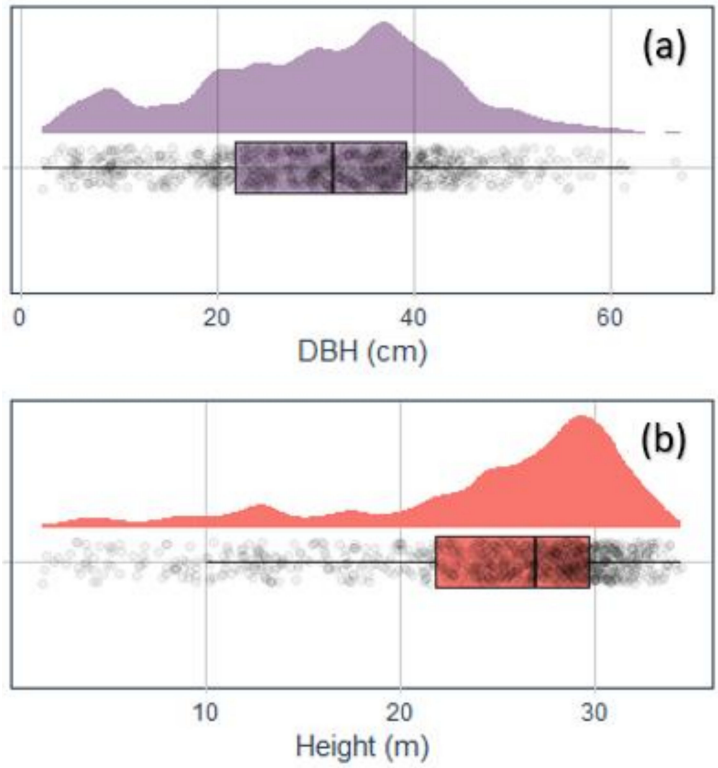

Figure 2. Plots showing the distribution of diameter (**a**) and height (**b**).

The stand is located on a very flat site and is regularly mowed for access. Consequently, it has very little understory, which is limited to small patches of low-growing blackberry between the lines of trees. The aim of this study was to assess the absolute accuracy of phenotypic measurements from laser-scanned point clouds against field measurements.

This site was, therefore, an ideal choice for this study, providing idealised conditions with little noise from understory or terrain undulations to confound the measurements.

Table 1. Tree height and diameter distributions of the studied trees.

No. Trees	DBH Range (cm)	Mean DBH (SD) (cm)	Height Range (m)	Mean Height (SD) (m)
884	2.2–67.1	30.5 (12.58)	1.7–34.4	23.9 (7.93)

2.1.2. Field Data

Ground validation for this study was carried out in the form of traditional forest mensuration. Pre-harvest inventory (PHI) was conducted on every tree within the stand following the PlotSafe methodology and utilising the RAD05 cruising dictionary commonly used in New Zealand [48]. Phenotypic traits were measured at the tree level and included DBH measured at 1.4 m, tree height, stem straightness, branch size, green crown height, and stem malformation. DBH was measured over bark to the nearest millimetre using a diameter tape, and heights were measured to the nearest 0.1 m with a Vertex 4 hypsometer (Haglöf, Langsele, Sweden). PHI was conducted between 12 and 16 October 2020. Due to the time elapsed between field measurements and laser scanning, DBH was re-measured between 11 and 13 August 2021. Any discrepancies found between these measurements and the field data were checked by remeasuring diameters in the field to avoid any anomalous results.

In addition to the mensuration data, a sub-sample of twelve trees was intensively measured using a crown-mapping procedure. For this exercise, an intensive phenotypic assessment was undertaken, including measurements of internodal diameters, internodal distances and whorl height above ground level (AGL) for the entire stem up to a height of 20 m. Heights and internodal measurements were measured by a crew of two certified climbers using a 50 m nylon measuring tape that was secured at the base of the tree and in the tree crown (Figure 3a). Internodal diameters were measured with a DBH tape.

Figure 3. Images from the data capture showing (**a**) measurements being recorded to a mobile application during crown mapping and (**b**) a target deployed to the site as a ground control point.

2.1.3. MLS Data

Ground-based lidar data were captured using the Hovermap MLS (Emesent, Milton, QLD, Australia) (Figure 4a). The Hovermap comprises a Velodyne Puck-LITE (VLP-16) laser scanner, which houses an array of 16 lasers that spin 360° about a single axis. The

scanner is mounted on a rotating arm, which allows the whole scanner to rotate about 360° on a perpendicular plane giving the unit full spherical 360° coverage while the system is in a stationary position. The system is SLAM-based, enabling the capture of coherent point clouds below the canopy, independent of GNSS signal availability. The Hovermap can be utilised in multiple formats, such as a handheld, backpack, vehicle-mounted or UAV-mounted MLS system. For this study, the backpack-mounted format was utilised.

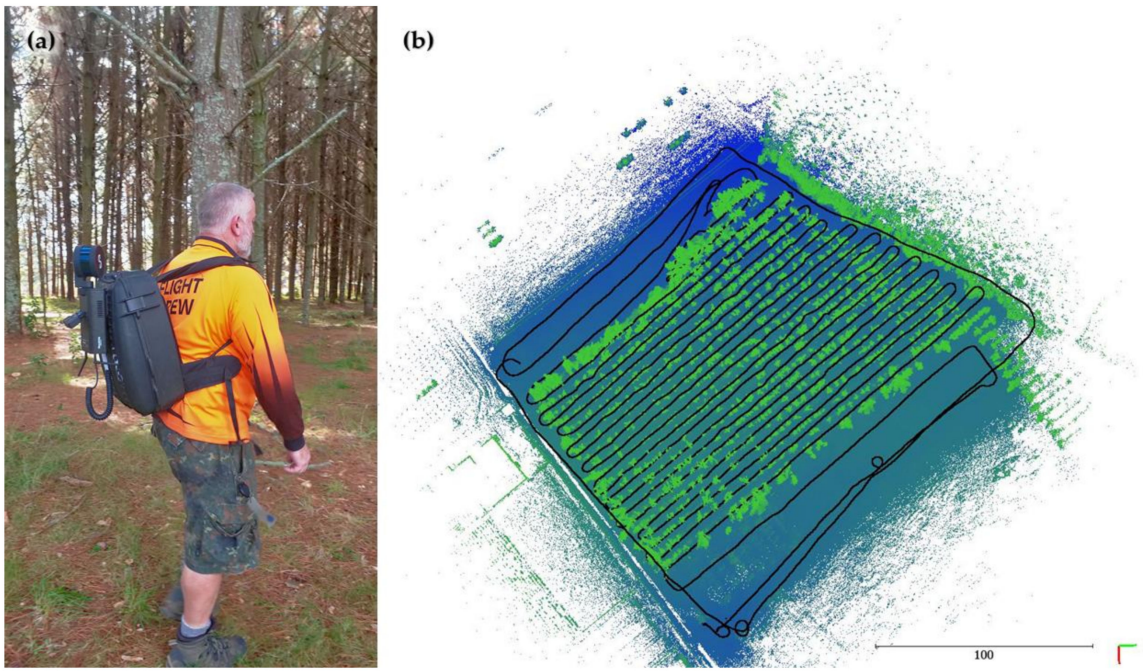

Figure 4. The Hovermap MLS in use (**a**) and (**b**) the trajectory of the MLS (in black) overlaid on stem locations within the trial, coloured by height (blue = low, green = high).

To create an accurate point cloud, the SLAM algorithm requires a process of "closing the loop" in which the scanner is required to regularly revisit areas previously scanned to aid in tying new scenes to the existing point cloud. The selected walking path conformed well with these specifications. The trajectory of the backpack capture plan is shown in Figure 4b. The MLS data capture was carried out on 28 July 2021 and resulted in a point cloud with a pulse density of 22,256 pulses per square metre (ppm^2).

2.1.4. ULS Data

ULS data for this study were captured using a LidarUSA snoopy V-series lidar system, with an integrated Riegl MiniVUX-1 UAV laser scanner. ULS data capture was carried out using a DJI Matrice 600 Pro hexacopter (DJI Ltd., Shenzen, China) (Figure 5b). The snoopy V-series is a PPK (post-processed kinematic) system that uses a CHCX900B base station (CHC Navigation, Shanghai, China) to log GNSS data to correct the UAV-mounted rover trajectory. The RMSE of the base station was 0.012 m.

Flight planning was undertaken using the UgCS flight controller software (SPH Engineering, Riga, Latvia). In line with recommendations from Wallace et al. [49], flights were carried out at 55 metres AGL to ensure a 20 m vertical separation between the tallest tree in the stand and the craft, whilst ensuring minimal beam divergence and higher point accuracy. The stand was flown in four directions with a 10-metre line-spacing between flight passes to increase pulse density and incidences of pulses penetrating gaps in the canopy. The first flight plan included flights both along and perpendicular to the rows of trees. This was then duplicated and rotated by 45° to create the second flight plan (Figure 5a). ULS data were captured on 5 May 2021 and the resulting point cloud had an average pulse density of 1818 ppm^2.

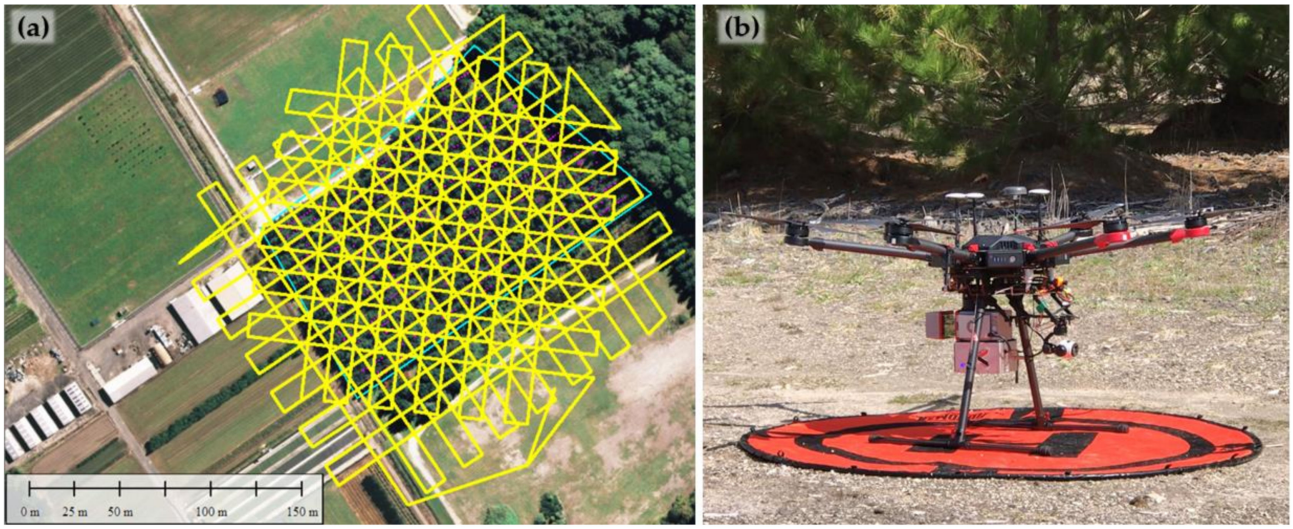

Figure 5. The flight plan for ULS data capture (**a**) and (**b**) image of the MiniVUX ULS mounted on the UAV system used in this study.

2.1.5. Ground Control: CloudReg

MLS data from the Hovermap backpack configuration does not contain GNSS data so it had to be georeferenced and aligned with ULS data. However, georeferencing the RS measurements using field measurements in mature forestry stands is traditionally a difficult exercise owing to the low accuracy of GNSS data captured beneath the forest canopy [36]. Therefore, Scion has developed a methodology called "CloudReg" to achieve highly accurate co-registration of airborne and terrestrial RS data sets. CloudReg allows for precise plot maps and, in turn, the confidence to enable tree-level comparisons of field and remotely sensed data sets.

Prior to data capture, ground control points (GCPs) were established on the open ground around the perimeter of the stand (Figure 1), utilising a Trimble Geo7X handheld GPS unit (Trimble Inc., Sunnyvale, CA, USA) with a Trimble Zephyr Model 2 external aerial. In this study, six 1 m^2 targets coated in highly reflective material (Figure 3b) were utilised as GCPs, remaining in place for both the ULS and MLS data captures. These targets were clearly visible within intensity-colourised ULS and MLS point clouds allowing for accurate co-registration of the data sets. The RMSE of the GCPs collected ranged from 0.05 m to 0.15 m.

Once the data were captured and the ULS and MLS point clouds processed, the two data sets were loaded into the CloudCompare software package (CloudCompare, version 2.12 alpha; CloudCompare, Paris, France). The point clouds were coloured by backscatter intensity values and co-registered by aligning the GCPs within both data sets using the 'Align (point pairs picking)' tool. After co-registration with the ULS point cloud, the overall RMSE of the MLS point cloud across the site was 0.27 m. Figure 6 shows a detailed view of a single tree point cloud from the ULS data each stage of the MLS data processing, as well as images of the co-registered point clouds.

2.2. Data Processing and Analysis

2.2.1. MLS Data Processing

Raw data files from the Hovermap were processed utilising the Emesent software package version 1.5 (Emesent, Milton, QLD, Australia). Data files were loaded into the software package, which then uses Emesent's proprietary SLAM algorithms to generate a point cloud in the LAS format. To increase the quality of matches, some parameters were adjusted from the defaults, including setting a spherical search radius of 1.5 m, a sliding window size of 8 s and 14 global iterations for registration.

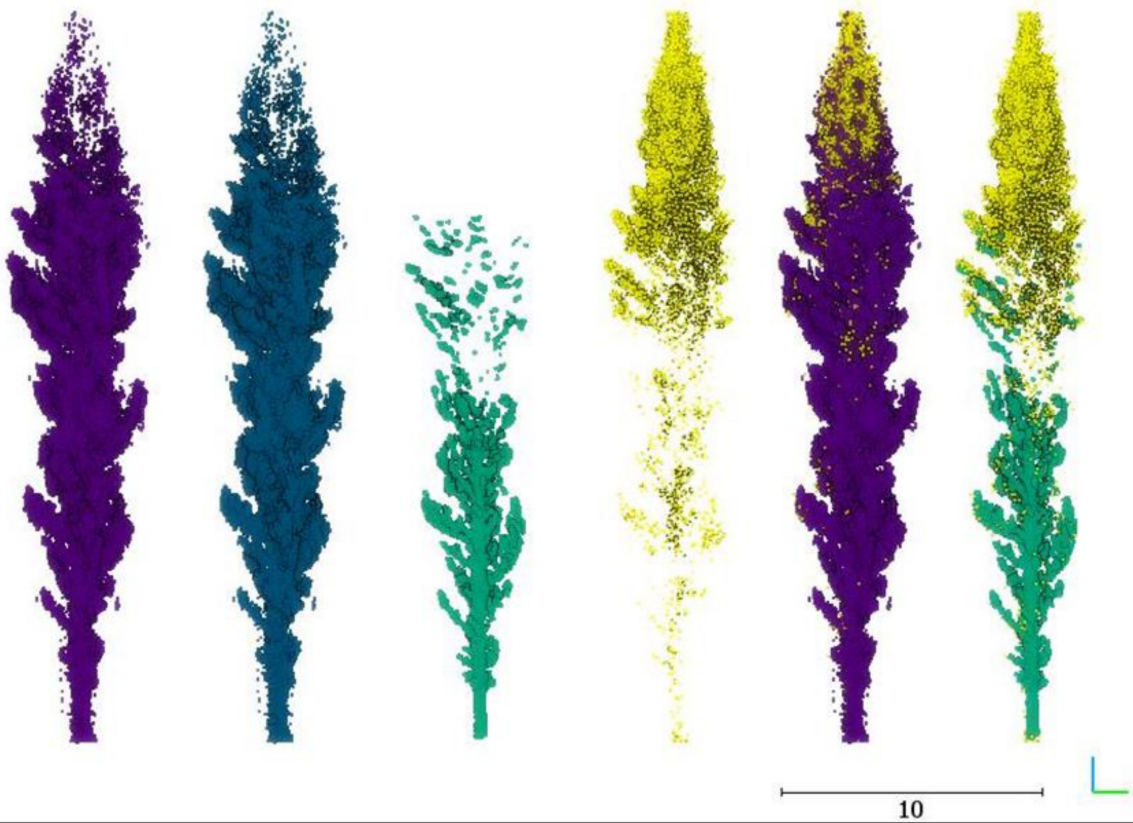

	Raw MLS	Decimated MLS	Output MLS from SimpleForest	ULS	Co-registered Raw MLS and ULS	Co-registered Output MLS and ULS
No. points	1,505,035	398,968	196,682	15,410	1,520,445	414,378

Figure 6. Detailed views of an individual tree point cloud (Tree F43) from the MLS and ULS data. MLS data are shown in their raw, decimated and processed forms. Figure also includes overlaid images of the co-registered raw MLS and ULS point clouds, demonstrating the similarities in maximum height and co-registered processed MLS and ULS point clouds. Number of points is reported below each model.

2.2.2. ULS Data Processing

To derive point clouds in the universal LAS data format, all ULS data were processed from the manufacturer's native data formats, utilising the Inertial Explorer (NovAtel Inc., Calgary, AB, Canada) and ScanLook PC (Fagerman Technologies, Inc., Somerville, AL, USA) software packages. The Snoopy V-Series system utilises a PPK GNSS system to enhance the accuracy of the output point clouds. As such processing involves two stages, the GNSS rover data were post-processed first, utilising the data from the GNSS base station within the Inertial Explorer software. During this initial step, filtering was also applied to remove noise points within a minimum distance from the scanner. Finally, the ScanLook PC software was used to apply boresight calibration angles and lever-arm offsets to the point cloud data, removing any inherent errors.

2.2.3. Individual Tree Segmentation

Co-registered MLS point clouds were imported to a segmentation pipeline developed utilising multiple algorithms within the SimpleForest software package [50]. For computational reasons, the large LAS files had to be tiled into smaller subregions. The segmentation pipeline consisted of four main steps: (i) ground classification and height normalisation, (ii) stem cloud generation, (iii) individual tree segmentation and (iv) segment post-processing.

In the first step of the segmentation pipeline, the imported point cloud was decimated using a point-distance-based method to reduce the point density to a manageable size. Ground points were classified and filtered using various denoising algorithms within the package. The point cloud was then normalised and divided into two sections, i.e., lower and upper clouds, using a vertical height threshold. A Euclidean clustering algorithm was applied to the lower cloud to detect clusters representing stem segments. These stem segments were then used as the seeds for the individual tree classification. Dijkstra [51] and Voronoi-based clustering methods were used to allocate the unclassified points in the upper point cloud to the seed stem segments. In the final step, various denoising algorithms, e.g., radius, statistical and Euclidean outlier filtering, were used to denoise the detected individual tree segments. A height-based tree identification filter was implemented to filter out shrubs, grass and other non-tree segments and the remaining individual tree segments were exported in LAS format.

The stem cloud generated in step two was used to create a stem map of the study site, which was later validated in the field using a GIS-based mapping app and field observations.

2.2.4. Derived Tree Form Metrics

Individual tree point cloud processing and tree metric derivation was carried out in the R statistical computing language [52]. The individual tree segments produced by the SimpleForest pipeline were imported as inputs to a stem delineation algorithm in the TreeLS library in R [53]. The detected stem points were then isolated and segmented into chunks using pre-defined height intervals (1, 2.5, 5, 10 and 20 cm). Two-step sphere fitting was used to avoid the errors coming from the stem noise. The first sphere fitting estimated the centre XY coordinates of the stem chunk. The distance from centre coordinates to each point was then calculated and a Laplace–Gauss distribution was fitted to the distance values. The second sphere fitting was implemented only on the points within 0.1–0.9 confidence levels of the Laplace–Gauss distribution. The fitting parameters of the second sphere fitting, including diameter, centre XY coordinates and fitting error, were exported to create a diameter profile of the stem. When the number of points was insufficient to fit a circle or sphere, an "NA" value was assigned to the parameters. The diameter profile was then utilised to derive phenotypic metrics, including DBH, stem height, volume and swellings in the stem (nodes).

For DBH measurements, it is common practice in NZ to move the measurement of the DBH height from 1.4 m by a maximum of $\pm$10 cm to avoid taking the measurement over a swelling. If the swelling persists within this $\pm$10 cm tolerance, DBH is calculated from measurements taken from two internodal sections at equal distances above and below the swollen 1.4 mark in what is termed a "split". Additional guidelines are followed when moving the DBH height along the stem to ensure accuracy and consistency of measurement [48]. These guidelines result in four DBH height classes, direct measurement (diameter taken at 1.4 m AGL), direct measurement for small swellings (DBH height shifted from 1.4 m by a maximum of $\pm$10 cm to avoid small swellings on the stem), split for large swellings (two diameter measurements taken at roughly equal distances above and below 1.4 m to avoid large swellings on the stem) and direct measurement for large swellings (when none of the above measurements are applicable). Following these guidelines, a variable breast height (VBH) estimation method that used six different stem diameter profiles (1, 2.5, 5, 10 and 20 cm) and six different tolerances (0.001, 0.5, 1, 1.5, 2 and 2.5 cm) was instigated when extracting DBH from individual tree segments. The tolerance represents the minimum change in stem diameter between neighbouring stem slices. 0.001 tolerance is referred to as "any change", hereafter. In addition, as a control, diameter extracted at a set height of 1.4 m above the DTM (fixed-height method) and at the heights identified for measurement by the field crew (field-height method) was also tested.

Tree heights calculated from the SimpleForest pipeline displayed a strong negative bias due to aggressive noise filtering. We, therefore, used the original co-registered MLS point cloud to assess the height accuracy. Tree height was derived using a peak detection

methodology. First, the stem map created in the SimpleForest pipeline was converted to a shapefile of the stem locations at ground level. A buffer of 1 m was applied to each of the stem circles and a new shapefile representing a search radius for the tree peak was created. Point clouds from the ULS and MLS were then ground classified, height normalised and noise filtered to remove spurious points above the canopy using the lidR package [54] in R. The maximum height within each polygon of search-radius shapefile was then extracted as the tree height.

For stem volume calculation, the stem was divided into 10 cm thick slices, from which diameter profiles were extracted. A volume calculation algorithm that moves up the stem profile by aggregating the individual volumes of stacked slices was developed to obtain total stem volume. The algorithm only aggregates consecutively stacked chunks and stops aggregating when it detects an "NA" in the stem profile, even if there are additional spheres above this gap (Figure 7a).

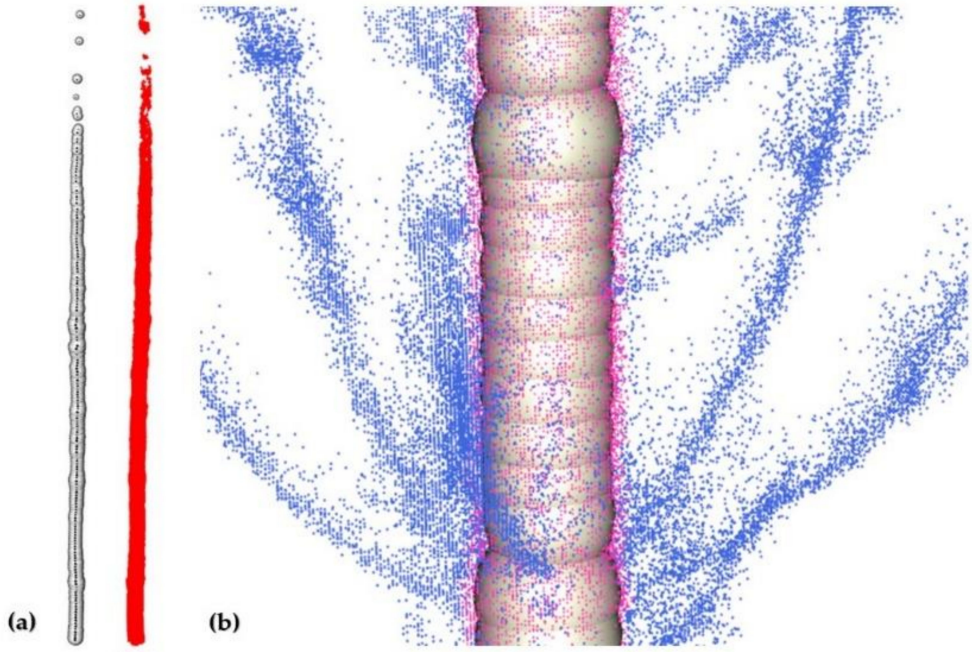

Figure 7. Images showing sphere fitting on a delineated tree stem. (**a**) Spheres of a whole tree stem (left) and stem points (right). (**b**) A close-up showing spheres (off-white), stem points (pink) and branch points (blue).

We used the stem diameter profiles (5/10/15 cm) of each tree to detect the segments that showed a significant increase in diameter compared with their neighbouring segments and marked them as potential nodal swellings (Figure 7b). The heights of these nodal swellings were later matched with field measured whorl heights.

2.2.5. Accuracy Statistics

Precision and bias were calculated using common statistical methods for the comparison of field and laser scanning metrics [5,24]. Root mean square error (RMSE) and mean bias error (MBE) are calculated as follows:

$$R^2 = \frac{\sum_i (\hat{y}_i - \overline{y})^2}{\sum_i (y_i - \overline{y})^2}$$

$$\mathrm{RMSE} = \sqrt{\frac{\sum_{i=1}^{n} (\hat{y}_i - y_i)^2}{n}}$$

$$\text{MBE} = \frac{1}{n}\sum_{i=1}^{n} y_i - \hat{y}_i$$

where y_i represents field measurements, $\hat{y}_i$ represents predicted measurements from point clouds, $\overline{y}$ is the average of the observed values and n represents the sample size. The relative RMSE (RMSE%) was calculated as the percentage of the average observed value: 100(RMSE/$\overline{y}$). To assess the impact of DBH on error, absolute error (AE) and percentage error (PE) were both calculated at the tree level. AE was calculated for each tree using the equation $|y_i - \hat{y}_i|$ and PE from $100 \times \text{AE}/y_i$. The effect of DBH on error was then evaluated by plotting AE and PE against DBH categories in bins with 5 cm increments from 0–65 cm.

The accuracy assessment of whorl detection was calculated as per Pyörälä et al. [45]:

$$Accuracy(\%) = \frac{n_a}{n_m + n_{fp}} \times 100$$

where n_a represents the number of correctly identified whorls, n_m represents the number of field-measured whorls and n_{fp} represents the number of falsely predicted whorls.

A confusion matrix was created for assessing the accuracy of DBH height class prediction by VBH method. The overall accuracy and kappa values were calculated using the confusion Matrix algorithm of caret package [55] in R statistical software environment.

3. Results

3.1. Individual Tree Segmentation

Of a total of 884 trees, 798 stems were correctly accurately segmented by the SimpleForest pipeline. This figure represents a detection accuracy of 90.3%. The trees that the algorithm failed to segment mainly consisted of trees with errors introduced in the tiling process (Figure 8b), trees that had low branching or were surrounded by denser understorey (Figure 8c,e,f) and the trees growing too close to a boundary fence. Trees that were very small or growing in clusters also caused greater incidences of segmentation failure (Figure 8d). Nearly 50% of the smaller diameter trees in clusters did not segment accurately.

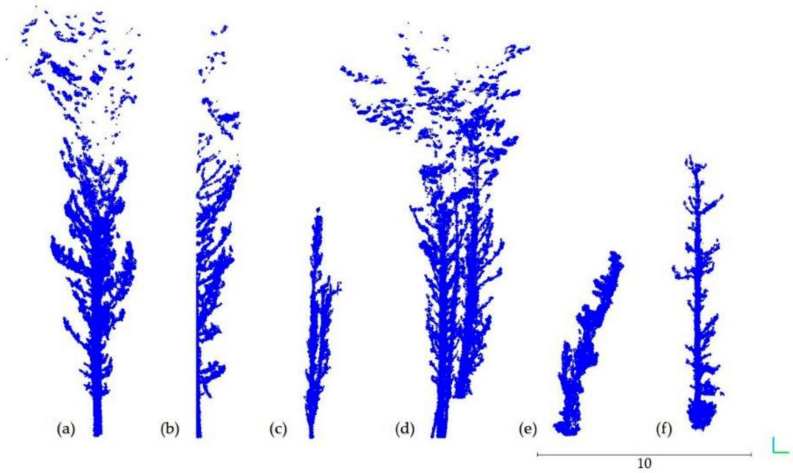

Figure 8. Selection of errors encountered in the segmentation process. (**a**) Tree F43—clear segmentation with accurate DBH; (**b**) tree D26—stem cut in half vertically in tiling process; (**c**) tree G4—forked tree with additional leader diverging from the main stem below DBH height; (**d**) tree O40—inclusion of more than one tree as a single segment; (**e**) tree G47—considerable needle noise at DBH height and (**f**) tree T41—understorey points attached to stem.

3.2. Tree Metrics

3.2.1. DBH

Overall, our results demonstrate high levels of correlation (R^2 = 0.96–0.99) and low levels of error (RMSE = 1.72–2.61 cm/5.4–8.2%) when assessed against field-measured DBH

(Figure 9). The best result for correlation (R^2 = 0.988) in our VBH diameter method was observed when the slice interval and tolerance parameters were set to 20 cm and "any change", respectively (Figure 10a); however, this method only achieved the fifth lowest RMSE (1.83 cm/5.8%). The lowest RMSE (1.72 cm/5.4%) was observed in the results for the DBH measurements taken at field height, with a 20 cm slice interval, which also has the third highest R^2 (0.987) (Figure 10b). The fixed height method, where DBH was derived at 1.4 m above the DTM, with a slice interval of 20 cm displays the third lowest RMSE (1.81 cm/5.7%) and fifth highest R^2 (Figure 10c). The optimal results from each of the three methods that were assessed: VBH method, the field-height method and the fixed-height method are shown in Figure 10.

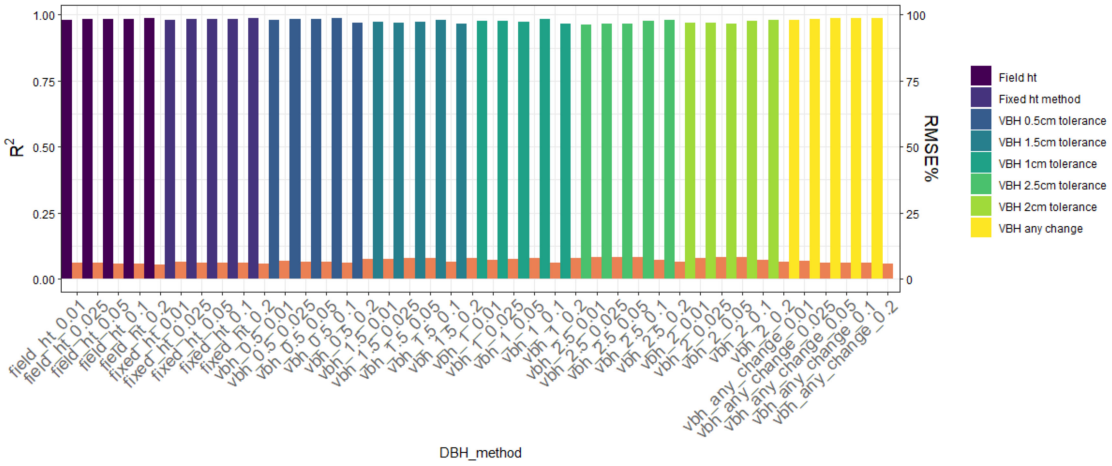

Figure 9. Correlation and relative RMSE values of each DBH methodology assessed. R^2 values represented by bars coloured by DBH method used, and relative RMSE represented by orange bars. The tolerance represents the minimum change in stem diameter between neighbouring stem slices, with tolerance of 0.001 referred to as "any change".

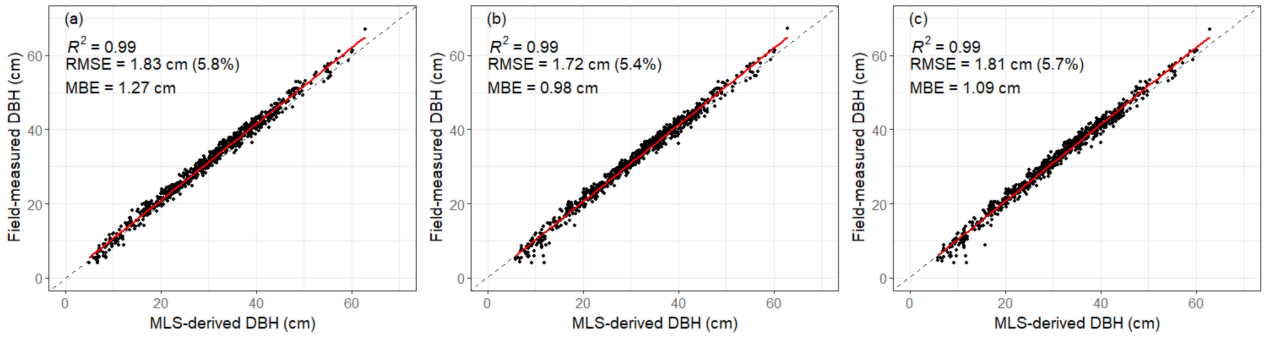

Figure 10. Correlation between field-measured and MLS-derived DBH. (**a**) The best MLS-derived DBH result from the VBH method, (**b**) the best result from the MLS measurements taken at field height and (**c**) the best result from the MLS measurements taken at a fixed height above the DTM. The dashed lines represent a 1:1 line and the red lines represent a fitted linear model with linear equation and R^2 shown.

When the sampled trees were binned into diameter intervals of 5 cm, trees with a DBH less than 10 cm show a larger AE (4.12–1.11 cm), which decreases with each group until the 15–20 cm group (1.07 cm) and then shows a trend for increasing positively with the increase in DBH (Figure 11b). PE, however, started high with the 0–5 cm DBH trees (~39%), decreasing to 5.5% in the 15–20 cm DBH group and then slowly decreasing incrementally to 2.1% in the 60–65% group, with minor fluctuations in the 35–40 cm and 50–55 cm groups (Figure 11a).

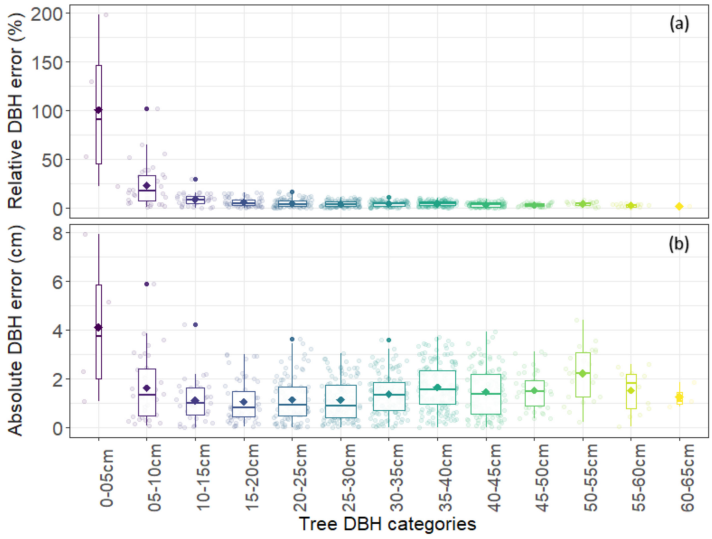

Figure 11. Variation of DBH categories in (**a**) MPE and (**b**) MAE between field-measured and MLS-measured values. Box plots show median error for each category and confidence intervals, with box width representing sample size. The mean error for each height class is represented by diamonds.

Generally, the performance of the VBH algorithm for predicting DBH height class was low to moderate with overall accuracy ranging from 34 to 52% for the different tunings of the VBH algorithm that we assessed, with the highest value observed for the VBH method with a 20 cm slice interval and any diameter change between neighbouring stem slices. Kappa coefficient values generally fell in the poor to slight agreement range, with the highest value of 0.143 observed by the same VBH model as the overall accuracy (Figure 12). When assessing the performance of DBH height class detection, the confusion matrix shows that the algorithm gives a moderate level of performance for taking a direct measurement at 1.4 m (58.8% correctly classified—recall) and moving for a small swelling (51.1.% correctly classified/recall) (Figure 13). A total of 36.6% of direct measurements were misclassified as small swellings, with 36.1% vice versa. The model performed poorly for split (3.5%), with 54.4% of splits being misclassified as direct measurements (Figure 13).

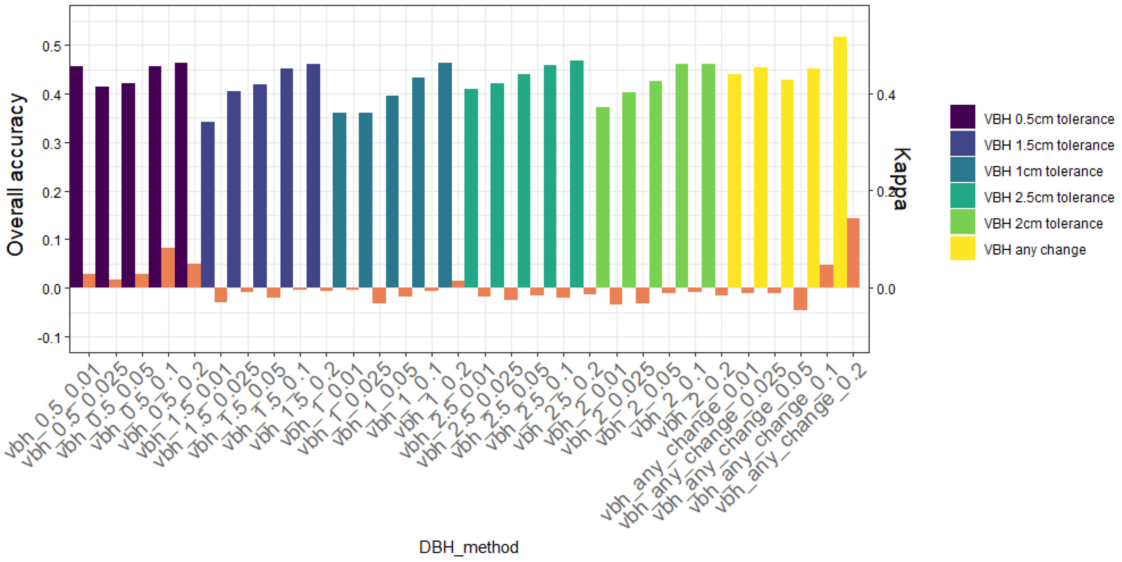

Figure 12. Accuracy and Kappa values for each of the VBH tunings that were assessed. Coloured bars represent overall accuracy of each tuning, coloured by the tuning of the tolerance; orange bars represent the kappa coefficient for each tuning.

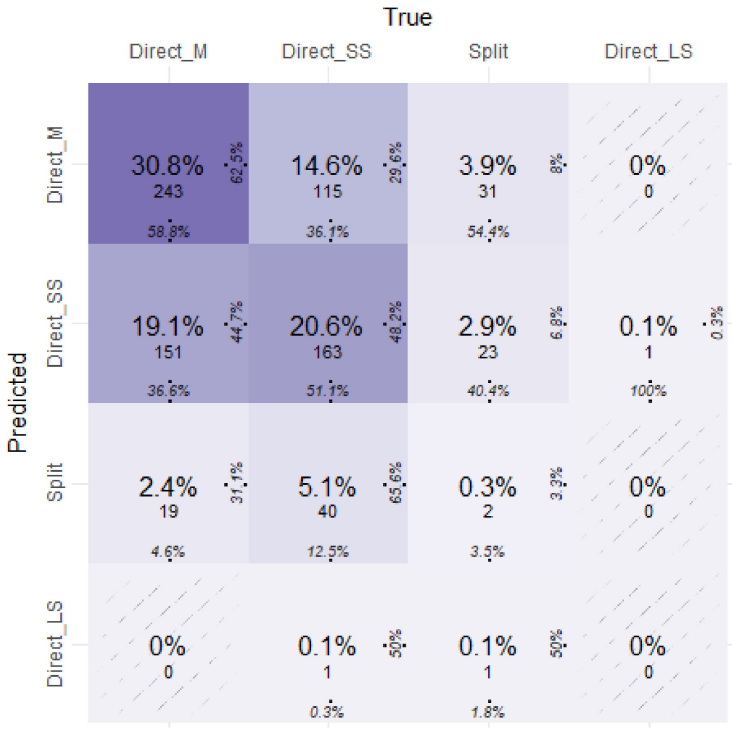

Figure 13. Confusion matrix showing the frequency that each DBH height class was identified by the VBH algorithm (expressed as a percentage with the number of occurrences below) and the percentage that each class was confused with a different class (small percentages), Direct_M is where a measurement was taken at 1.4 m (no swelling), Direct_SS is where the DBH was moved by <10 cm to avoid a small swelling, Split is where a split measurement was used to avoid a large swelling and Direct_LS is where a large swelling was too large to use a split and so a single measurement was taken at <1.4 m.

3.2.2. Tree Height

Both ULS and MLS height show a relatively weak correlation with field-measured height (R^2 = 0.24 and 0.22, respectively) (Figure 14a,c). The RMSE is also high for both scanners (at ~28.6%) with a mean bias of −3.57 m for the ULS and −3.46 m for the MLS (Table 2). Further analysis highlighted that most of the significantly over-estimated heights were attributed to suppressed trees, or trees with broken tops. After removing suppressed (which were measuring <20 m in height within the field data) and broken trees (which were recorded as broken during field visits) from the analyses, correlation with field measurements increased to 0.42 for ULS and 0.41 for MLS (Figure 14b,d) data. The improvements to RMSE and MBE stood at 10.14% and −1.32 m for ULS and 9.9% and −1.18 m for MLS (Table 2) data. The correlation between the heights derived from ULS and MLS data is very strong, with an R^2 value of 0.94 (Figure 15), an RMSE of 3.02% and an MBE of 0.11 m (Table 2).

Table 2. Accuracy comparisons between point cloud-derived height and field-measured height.

Variables	R^2	RMSE (m)	RMSE (%)	MBE (m)
ULS vs. Field	0.24	7.19	28.60	−3.57
ULS vs. Field (minus suppressed)	0.42	2.85	10.14	−1.32
MLS vs. Field	0.22	7.19	28.57	−3.46
MLS vs. Field (minus suppressed)	0.41	2.78	9.90	−1.18
ULS vs. MLS	0.94	0.87	3.02	0.11

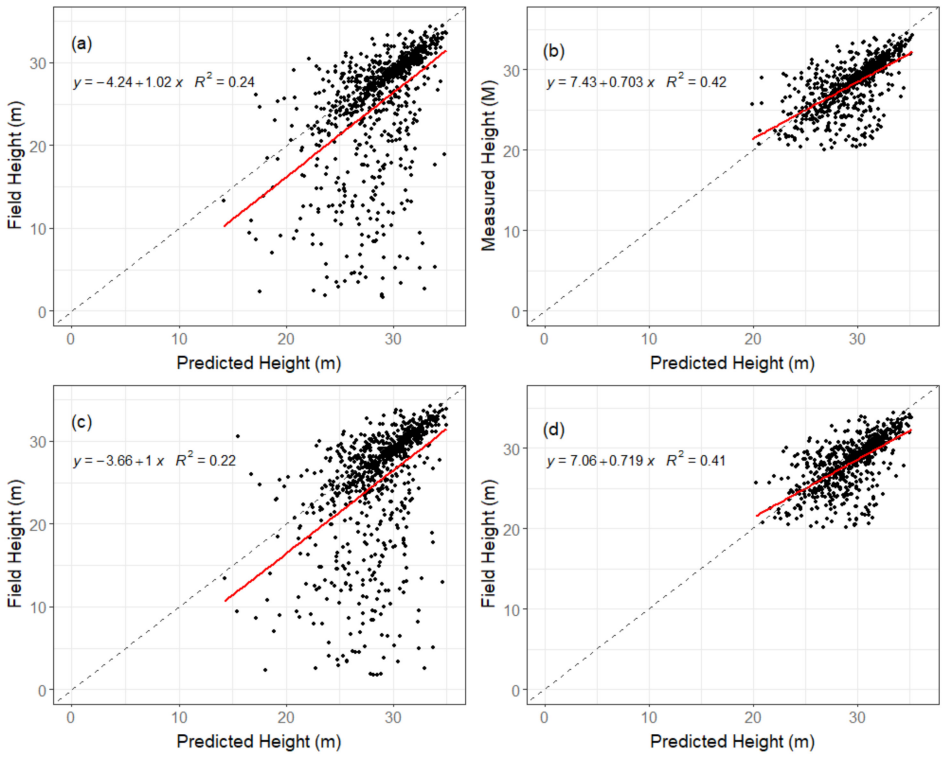

Figure 14. Correlation between field-measured and (**a**) all ULS-derived heights, (**b**) all MLS-derived heights, (**c**) ULS-derived heights with all suppressed trees removed and (**d**) MLS-derived heights with all suppressed trees removed. The dashed lines represent a 1:1 line and the red lines represent a fitted linear model with the linear equation and R^2.

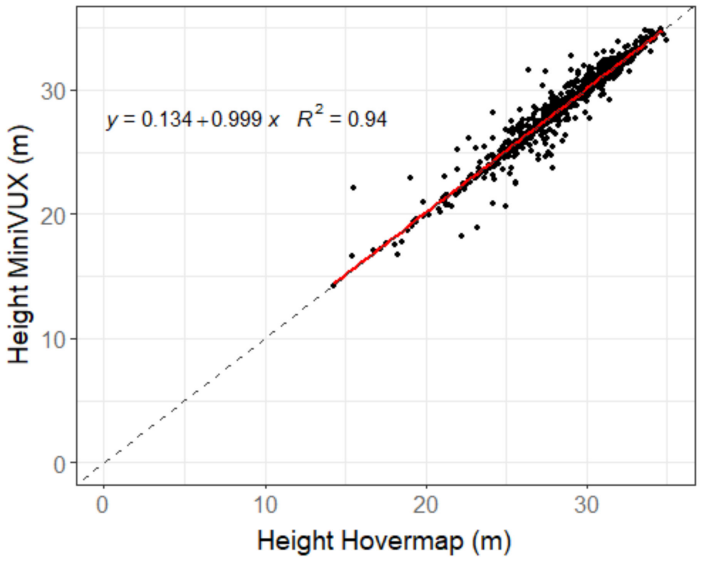

Figure 15. Correlation between ULS- and MLS-derived heights. The dashed line represents a 1:1 line and the red line represents a fitted linear model with the linear equation and R^2.

3.2.3. Stem Volume

Stem volume estimates from the MLS data show a very strong correlation with field-measured volume with an R^2 of 0.99 (Figure 16). The results show an RMSE of 0.21 m^3 (10.16%), with an MBE of 0.16 m^3. Sphere-fitting failures occurred at various heights for the trees assessed (Table 3). Consequently, stem volume is directly linked to the height up to which the algorithm was able to calculate volume.

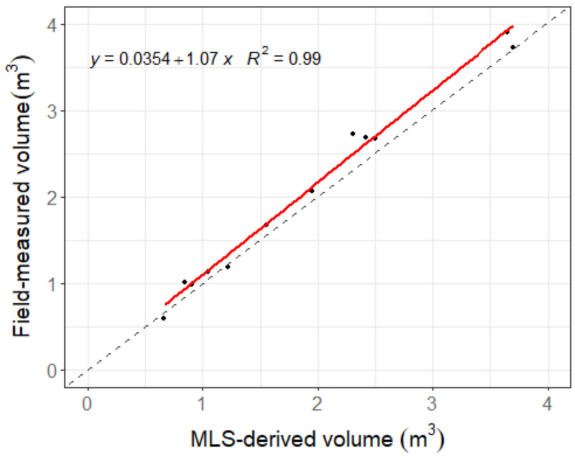

Figure 16. Relationship between field-measured volume and MLS-derived volume. The dashed line represents a 1:1 line and the red line represents a fitted linear model with linear equation and R^2.

Table 3. Tree-level volumetric calculations and whorl detection from MLS data. Results include the maximum height of stem included in the volume calculations, calculated stem volume, and the height of the highest whorl detected for 5 cm, 10 cm and 20 cm interval diameter profiles.

	Individual Tree Identifier											
	A8	**B23**	**C7**	**D14**	**E8**	**F19**	**G18**	**H7**	**J5**	**K1**	**L8**	**M7**
Max Ht (m)	13.9	14.0	10.5	10.10	17.9	10.8	12.9	9.1	17.1	15.8	18.9	17.9
Stem volume (m^3)	2.77	1.59	0.99	0.97	2.15	1.03	1.27	0.69	2.69	3.80	3.90	2.80
Max Ht Whorl (5 cm)	15.38	16.03	13.18	16.38	17.63	16.68	16.73	14.73	13.78	15.43	18.48	17.48
Max Ht Whorl (10 cm)	16.1	16.9	15.4	18.1	17.5	18.8	18.1	13.51	17.1	15.9	18.6	17.6
Max Ht Whorl (20 cm)	16.15	17.15	15.15	19.15	18.75	18.95	18.75	15.16	17.15	16.35	18.55	19.35

3.2.4. Whorl Detection

Whorl detection was analysed in two ways. First, the accuracy of whorl height measurements as detected by the algorithm was assessed via a linear regression (Figure 17). This involved assessment of true positive whorl predictions only. Second, the ability of the algorithm to correctly identify whorls on each tree stem was assessed. The algorithm assesses the stem diameters, averaged over a specified stem length, with neighbouring stem diameters. The algorithm was tuned to 5 cm, 10 cm and 20 cm stem slices.

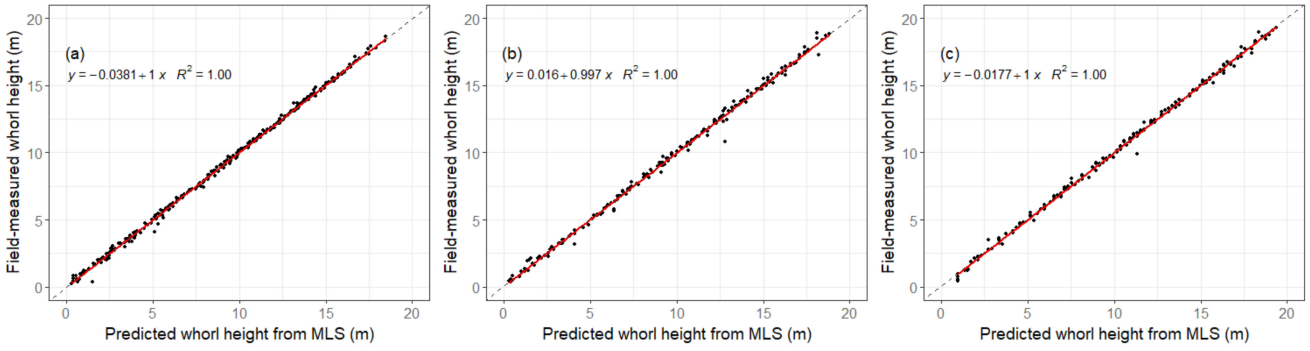

Figure 17. Relationship between field-measured whorl height and correctly detected whorl heights derived from the MLS data with (**a**) 5 cm, (**b**) 10 cm and (**c**) 20 cm configuration. The dashed lines represent a 1:1 line and the red lines represent a fitted linear model with linear equation and R^2.

All three settings of the algorithm returned a high level of precision, with RMSE values ranging from 17 cm/1.88% to 26 cm/2.73%) and a low level of bias, with all three tunings

showing an MBE of ~1 cm (Table 4). The detection accuracy was, however, only moderate, ranging from 40.25% for the 5 cm tuning to 42.41% for the 10 cm tuning (Table 4). The 20 cm configuration was able to characterise branches higher up the stem to a mean height of 17.55 m and a maximum of 19.35 m, compared with a mean of 16.97 m and maximum of 18.8 m for the 10 cm configuration, and 15.99 m and 18.48 m for the 5 cm configuration (Table 3).

Table 4. Results for whorl detection along with values for precision and bias for each of the three configurations of the detection algorithm.

Tuning (cm)	No. Whorls Measured	No. Whorls Detected	No. True Positives	No. False Positives	No. False Negatives	RMSE (m)	RMSE (%)	MBE (m)	Detection Accuracy (%)
5	410	602	289	313	108	0.17	1.88	−0.01	40.25
10	410	265	201	64	209	0.26	2.73	−0.01	42.41
20	410	193	175	18	235	0.22	2.10	−0.01	40.89

4. Discussion

In this study, a comprehensive ultra-high-density lidar data set was successfully captured using ULS and MLS technologies. The CloudReg methodology enabled the accurate co-registration and combination of the field, ULS and MLS data at the individual tree level, which to the best of our knowledge was not previously undertaken on this scale. Ancillary field measurements from crown mapping allowed for more intense scrutiny of metrics derived from below-canopy laser scanning proving the ability of MLS technology to characterise fine details of tree form. The results of our study show promise for the use of high-density MLS technology in extracting metrics for tree phenotyping.

4.1. Individual Tree Segmentation

In this study, we were able to segment 90.3% of the stand using an automated individual tree segmentation pipeline. These results are comparable to previous studies, reporting 92.4–94% segmentation rates for TLS in leaf-off conditions and MLS in leaf-on conditions, respectively [56]. Our results also show a marked improvement on previous studies using SimpleTree, a precursive software to SimpleForest for segmentation that achieved detection rates of 74% [57] and 58% (averaged across two plots) [28]. Previous studies found difficulties in segmenting trees with diameters of <10 cm [25,26]. The results show that our study suffered from similar issues with small trees, where 79 had a DBH of <10 cm which contributed to some of the segmentation failures. Of these, 63 trees were stunted and growing in un-thinned clusters. The rigorous filtering applied in the stem seed detection step may have removed a large number of smaller diameter trees that were in close association with larger trees. The stand was planted in a 1.5 m × 5 m spacing and never systematically thinned, resulting in areas of high stem density which caused some additional issues for the segmentation algorithm. These results suggest that future work should focus on resolving the segmentation of smaller trees and refining stem delineation in dense and un-thinned stands.

4.2. Tree Metrics

4.2.1. DBH

Previous studies suggested that the estimation of DBH at a fixed height above the derived DTM could potentially introduce errors, as the DTM averages the forest floor height [24]. The results of this study, however, show that there is no significant difference between using DBH measurements taken at a set height above a DTM, adjusting DBH heights to match field-measurement heights or by using a variable height algorithm to avoid areas of swelling on the stem. Diameter estimated using our VBH algorithm has a marginally stronger correlation; however, the lowest RMSE was observed when diameter was extracted from MLS data at field measured heights (Figure 10b). The fixed-height

method also displays lower RMSE than the VBH method (Figure 10c). However, the diameter results for the VBH, field height and fixed height methods were not significantly different at the 95% confidence level ($p = 0.0001$), which indicates that use of any of these methods for the measurement of plantation species, such as *P. radiata*, will give comparable results on flat terrain. Nevertheless, the results of our VBH methodology for accurately detecting swelling are moderate overall (52%), so further work should look to optimise this method, as this could further increase the accuracy of the VBH methodology. As our research was confined to a very flat site, we cannot be sure that steeper terrain will not influence the choice of algorithm and so further research should look to apply these algorithms in varied levels of terrain.

Some clear trends could be observed with the parameter tuning of our VBH algorithm, notably that the 20 cm slice interval delivered the best overall performance in all three methodologies, whereas using a 1 cm slice produced the weakest results. The performance of the 1 cm slice interval could be explained by a greatly reduced number of stem points in the slice after noise filtering. There is no clear pattern to explain the relationship between the thickness of the slice used for the DBH measurement and the threshold to detect swelling; however, this is an aspect that would benefit from future study to optimise this methodology.

The high level of correlation and RMSE we found between field-measured and our optimal MLS-derived DBH ($R^2 = 0.99$, RMSE = 1.72 cm/5.4%) conforms with the correlations reported in other SLAM-based MLS studies ($R^2 = 0.99$, RMSE = 1.11–2.9 cm/3.4–23%) [24,58]. Furthermore, our results fall within the upper end of studies focused more generally on TLS (R^2 range of 0.93–0.99 and RMSE = 1.13–3.37 cm/5.4–13.4%) [24,26,58–61]. MLS-derived DBH displayed a negative bias of ~1 cm, which was most pronounced in trees of larger diameter. When exploring this further, our results showed that the percentage error is negatively correlated with DBH, with a notable increase for trees < 15 cm in diameter. However, our results also show that the absolute error, although higher for trees less than 10 cm, slowly increased from an MAE of ~1 cm with trees of 10–20 cm up to ~2 cm in the 50–60 cm diameter range. Other studies also observed this and proposed various explanations, including the decreased accuracy due to the roughness of the bark [24,25,62] and the prevalence of stem profile irregularities in older trees [24]. Our results confirm the findings from previous studies [24,25,58], which indicate that trees with a diameter of <10 cm show higher levels of error in the MLS data. Smaller diameter *P. radiata* trees are more likely to have lower branches and, therefore, in this study, we found more noise around the DBH height (see Figure 18c,e) of smaller diameter trees, which other studies also reported for different species [24]. Additional errors can also arise from segmentation errors that exclude part of the stem (Figure 18b) or include additional stems or understorey (Figure 18d,f). Our results imply that the Hovermap MLS scanner would give the best DBH results for trees in the 10–20 cm diameter range, but future studies should focus on assessing this relationship more closely.

The accuracy of the VBH algorithm in determining DBH height class was moderate, with the optimal tuning delivering an overall accuracy of 52% (Figure 13). Our findings demonstrate that the thickness of the stem slice used to derive DBH has an impact on the accuracy of the model, with 20 cm providing the optimal model, and also on the tolerance for identifying swelling, demonstrating some impact. The low Kappa scores, however, indicate that the model performs poorly in identifying swelling (Figure 12). This lack of accuracy could be related to the aggressive point filtering of the stem-delineation pipeline, which could mask some of the stem swelling. Future research should focus on fine-tuning our approach to make the variable height algorithm more sensitive to swellings of difference sizes.

Other reasons for the differences in DBH measurements could be related to the accuracy of field measurements. Although the utmost care was taken to ensure the accuracy of measurements, human error cannot be discounted from the field measurements and some obvious errors were noted and remeasured. Field measurements involve an element of

subjectivity in deciding where to measure the DBH and determining the highest ground point from which to take the 1.4 m from. Grass and leaf litter could also add noise to the DTM, a factor that would not impact field measurements as an inventory forester would ensure that the height pole was sighted on solid ground. To avoid this scenario, other studies compared MLS data with TLS data [22,24,25].

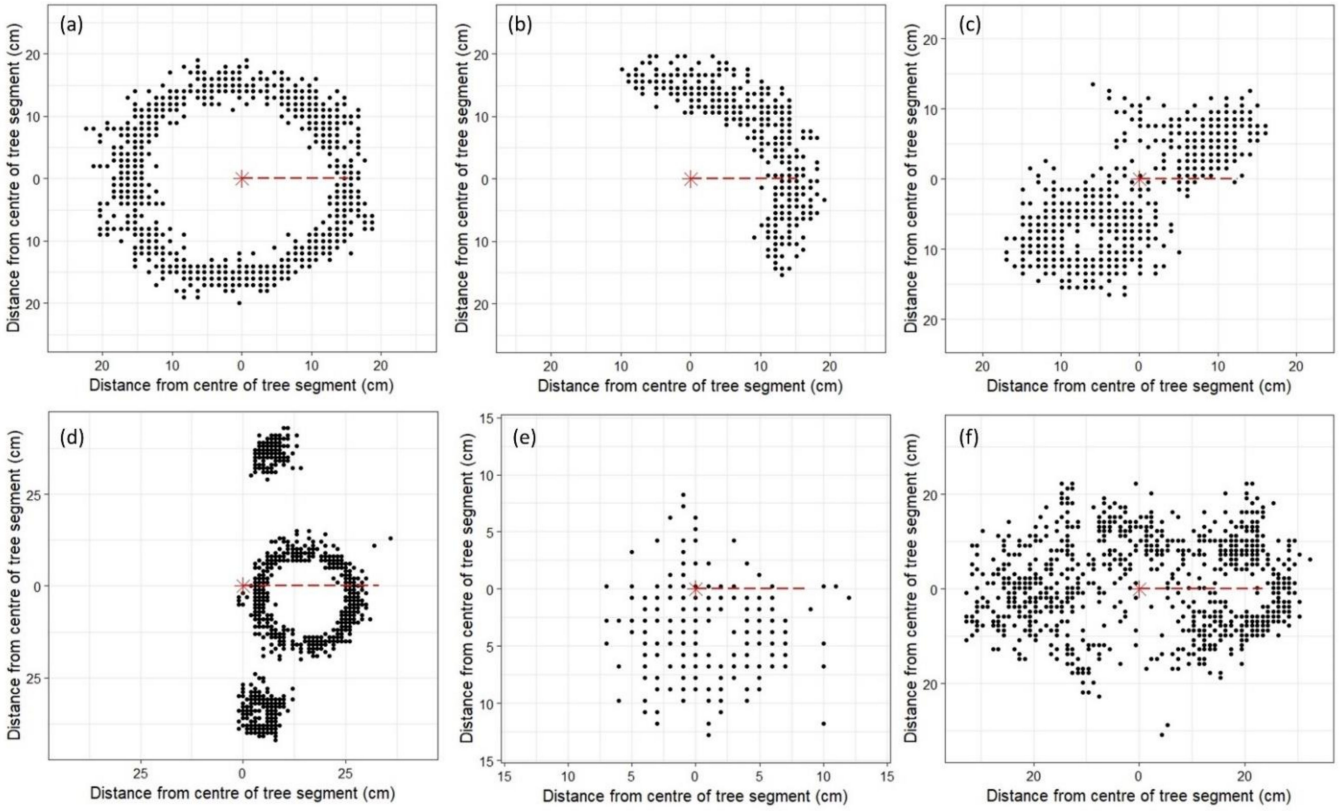

Figure 18. Stem cross-sections at DBH height, with red cross denoting estimated centre point from sphere fitting and red dashed line showing the estimated radius. Cross-sections align with profiles from Figure 7: (**a**) tree F43—clear segmentation with accurate DBH, (**b**) tree D26—stem cut in half vertically by tiling errors, (**c**) tree G4—forked tree with additional leader diverging from main stem below DBH height, (**d**) tree O40—inclusion of more than one tree as a single segment, (**e**) tree G47—considerable needle noise at DBH height and (**f**) tree T41—understorey points attached to stem.

4.2.2. Height

The accuracies of MLS-derived (R^2 = 0.22/RMSE = 7.19 m/28.57%) and the ULS-derived (R^2 = 0.24/RMSE of 7.9 m/28.6%) height were relatively low. When compared with the literature, this is unusually weak with previous studies on TLS reporting RMSEs between 0.54 m and 6 m [39,63–67] and R^2 values between 0.57 and 0.95 [63,64,67]. ULS height was also reported to have much higher R^2 (ranging from 0.76 to 0.97) [68–72] and RMSE (0.72% to 7.91%) [26,68,70,71,73] values. The poor results can largely be attributed to the overestimation of height for suppressed trees within the stand. Figure 19 shows an example of two suppressed trees that were overestimated by ~15 m by both scanners.

When the suppressed and broken trees were removed from the results, we observed significant improvements in agreement (R^2 = 0.42 and 0.41) and precision (RMSE = 2.85 m/10.14% and 2.78 m/9.9%) for the ULS and MLS scanners, respectively. These results are consistent with findings of a previous study, which found a much higher level of precision with unbroken trees (RMSE = 6.8%) compared with broken trees (RMSE = 56%), the inclusion of which significantly affected overall precision (RMSE = 15%) [36].

The negative effect of suppressed trees on the results implies that the peak detection method used in this study is not appropriate for single tree-level height measurement in

mature stands. Alternative methods for tree height detection were proposed to compensate for this [74] and future studies should look to apply these algorithms to MLS and ULS data at an individual tree level to assess their efficacy.

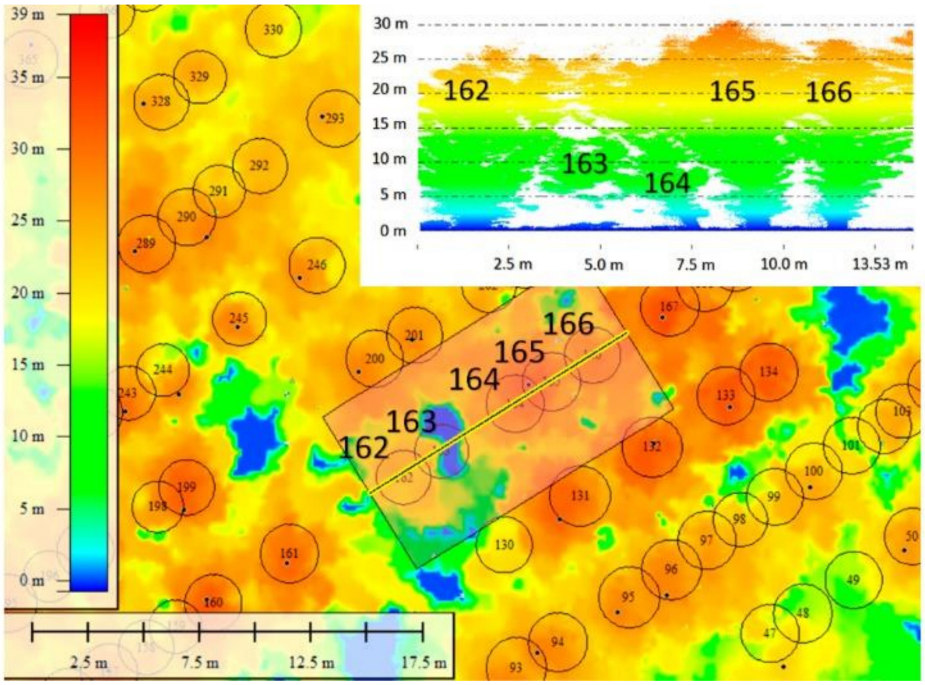

Figure 19. Nadir view of two suppressed trees in the CHM, and inset as a transect, highlighting the issue of using peak-detection for suppressed trees.

Due to delays in the project caused by COVID-19, the ULS and MLS data sets were captured 9 months and 11 months, respectively, after the field data. The potential impact of this time lag between data captures must also be considered. Comparisons with a prior ULS data capture of the site reveal an average 1.45 m increase in peak height from May 2020 to May 2021. Additionally, tree height is notoriously difficult to capture in the field and even an experienced mensuration forester can have trouble accurately attaining height due to occlusion, tree lean or inter-twined treetops [75,76].

To remove time lag between measurements and other potential sources of error and to assess the absolute accuracy of MLS height, we compared the MLS-derived height to ULS-derived height, as our previous study reported a very high level of accuracy (R^2 = 0.99, RMSE = 5.91%) in tree height of *P. radiata* stands [5] using ULS data. The results were extremely encouraging, demonstrating a strong correlation (R^2 = 0.94) and a lower RMSE (0.87 m). Interestingly, the MBE of 11 cm between the two scanners indicates that the MLS data overestimated the tree height. Once the issues with measuring individual tree-level heights are resolved, this would also suggest that the MLS data captures the height of mature trees with sufficient accuracy to negate the need for capturing ULS data from the air. This is a significant finding, as previous research has indicated that TLS and MLS are both prone to underestimation of tree height due to the low range of the scanners and the occlusion caused by branching [22].

4.2.3. Stem Volume

The stem volume assessment found that the MLS volume estimates were very strongly correlated with field measurements (R^2 = 0.99). Estimates demonstrate a moderately high level of precision (RMSE = 0.21 m^3/10.16%) and a tendency to underestimate volumes (MBE = 0.16 m^3). These findings fit well with existing studies that showed underestimation of between 6.8% and 15% of total stem volume [26,42,77,78]. Of these studies, the closest

methodology to that used in this study reported a general underestimation of stem volume of up to 10% when comparing TLS with destructive sampling methods [42].

There was a slight inversely proportionate decrease in accuracy with an increase in total stem volume (Figure 16). As expected, the volume per tree was related to the height up the stem to which our algorithm was able to derive volume (Table 3). One possible reason for this increase in volumetric error could be associated with an increase in the diametric error of the point cloud higher up the stem caused by decreasing point density. This would manifest itself as a greater error in tree volumes that include a greater proportion of stem length. This is not an uncommon phenomenon and was observed in other studies that used TLS and ULS data [34,66,79,80].

On average, the volumetric algorithms deployed in this study were able to calculate volumes up to ~14 m, with a minimum and maximum height of 9.1 m and 18.9 m. In their study, Bruggisser et al. [34] calculated that 71.9% of total stem volume could be found within the first 10 m of the stem. Using this logic, measurements from the MLS should be able to account for a minimum of two-thirds of the tree's volume with an accuracy of ~90%. This is a significant finding when the measurement of DBH, particularly in smaller trees, is inherently biased with this technology. DBH is a measurement developed to standardise tree growth assessment in a practical and convenient manner, and can be used for calculation of stem volume, alongside measurements for tree height and taper equations. The ability to calculate stem volume directly from the stem profile removes the need for this legacy measurement and would arguably result in more accurate results for stand volume. Future research should be focused on better understanding the interaction between stem curve and diametric error for the MLS data. A better understanding of this relationship, along with the development of methods to derive volume from areas of the stem point cloud with lower point density, could aid in the development of usable models for deriving stem volume from MLS point clouds.

4.2.4. Whorl Detection

All three configurations of the whorl detection algorithm showed high levels of precision (Figure 17) and correlation with field measurements (Table 4) for whorl height when manually aligned. The whorl detection algorithm also outperformed the volume calculation algorithm in terms of the proportion of the stem covered (Table 4), with the best configuration (20 cm) detecting whorls up to a max height of 19.35 m and a mean height of 17.55 m. This is likely because the sphere-fitting algorithm struggled to fit spheres to smaller chunks (e.g., 10 cm) of the stem higher up the tree (see Figure 7).

The whorl detection accuracy was somewhat lower than the whorl height accuracy. The highest and lowest accuracies were achieved by the 10 cm (42.41%) and 5 cm (40.25%) configurations, with false-positive rates of ~24% and ~52%, respectively. The 5 cm configuration was able to correctly identify the most whorls (~70%); however, it also generated nearly fivefold more false positives than the best configuration. Similar work by Pyörälä et al. [45] used clusters of detected branches to identify whorl locations on the stem. Their algorithm correctly detected only slightly more whorls than the algorithm in this study, at 71.1%; however, the low number of false positives (1.9%) increased the overall detection accuracy to 69.9% (compared with 40–42% in this study). Possible reasons for this large difference in detection could be due to their use of TLS, which is known to create less noisy point clouds than the MLS system used in this study [29]. Their reported mean lowest whorl height was also above 7 m high, with a maximum lowest whorl height of 13.5 m, due to self-pruning of the studied species. This would indicate that their stems had fewer branches, thus much less noise than the *P. radiata* in our study, which was pruned up to ~2 m. Future studies should be focused on methods for reducing the number of false positives identified in our method, possibly by integrating branch and stem swelling detection to improve overall accuracy.

5. Conclusions

Unlike earlier stages of the forest-growing process, mature forests are challenging to segment and characterise owing to the dense, multi-layered canopy and the height of the trees. This study has shown that accurate phenotypic measurements can be derived from mature stands of *P. radiata* using Mobile Laser Scanning (MLS) units, such as the Hovermap. From MLS point clouds, a range of measurements, including diameter at breast height (DBH) and stem volume can be extracted with a high level of agreement. When combined with the CloudReg approach, the segmentation pipeline implemented in this study enabled highly accurate segmentation and tree location identification, demonstrating the scalability of MLS for phenotyping operations.

The novel variable height method introduced for determining measurement height for DBH performed moderately for avoiding swelling. The method did, however, perform strongly for the estimation of DBH when compared with the existing methods in the literature, deriving measurements with low levels of RMSE.

A key finding of this study is that, from the ground, the MLS can derive canopy height with a level of precision and accuracy comparable to a high-end ULS from the air. Despite needing more work to increase accuracy at the individual tree-level, this finding has significant implications for forestry as it was previously necessary to use laser scanners both above and below the forest canopy to estimate tree height and characterise stems from the same point cloud.

Volume extraction from the MLS data showed high levels of precision and, despite occlusion of the upper stem, and showed promise as a potential replacement for legacy measurements involving DBH and height.

The whorl detection method proposed in this study and its results establish a benchmark for more advanced methods of whorl detection and branch characterisation.

Measurement of smaller, suppressed trees were particularly problematic for both diameter and height measurement from the MLS data. However, overall MLS technology holds significant potential as a means of advancing phenotyping, forest mensuration and inventory at different scales, particularly for characterising fine details in tree form when used in combination with fine-tuned and standardised metric extraction algorithms. Thus, further research should focus on testing MLS tools in more diverse forest environments, refining capture techniques for better characterisation of the upper stem and fine-tuning algorithms to further increase the accuracy and precision of measurement.

Author Contributions: Conceptualization, R.J.L.H. and S.J.; methodology, R.J.L.H. and S.J.; formal analysis, S.J., R.J.L.H., S.J.D. and A.W.; investigation, R.J.L.H. and S.J.; resources, R.J.L.H. and G.D.P.; data curation, P.D.M., R.J.L.H., D.D.S. and H.J.E.; writing—original draft preparation, R.J.L.H.; writing—review and editing, S.J., R.J.L.H., A.W. and G.D.P.; visualization, R.J.L.H. and S.J.; supervision, R.J.L.H.; project administration, R.J.L.H.; funding acquisition, R.J.L.H., S.J. and G.D.P. All authors have read and agreed to the published version of the manuscript.

Funding: This research was funded by Scion's Strategic Science Investment Funding (SSIF) provided by the Ministry of Business Innovation and Employment (MBIE). Additional co-funding was provided by the Forest Growers Levy Trust and the MBIE Transforming Tree Phenotyping programme (C04X2101).

Data Availability Statement: The data presented in this study are available on request from the corresponding author. The data are not publicly available due to the large size of the data files and for privacy reasons.

Acknowledgments: We would like to thank Andy Neverman for his tree-climbing expertise to help design and deploy climbing methods for crown mapping, along with Gancho Slavov and Peter Bird of Scion for their assistance in collecting the crown-mapping data. We would like to acknowledge Liam Wright from NIWA (formerly of Scion) for his assistance with Hovermap data capture in the wider project. We would also like to thank Alan Tan (NIWA, formerly Scion) and David Pont (Scion) for their involvement in the development of this project. We would also like to acknowledge Forest

and Woodlot Inventory Services for capture of the mensuration data for this study. We thank Jan Hackenberg for his help with the SimpleForest individual tree segmentation script.

Conflicts of Interest: The authors declare no conflict of interest. The funders had no role in the design of the study; in the collection, analyses, or interpretation of data; in the writing of the manuscript, or in the decision to publish the results.

References

1. Costa, C.; Schurr, U.; Loreto, F.; Menesatti, P.; Carpentier, S. Plant phenotyping research trends, a science mapping approach. *Front. Plant Sci.* **2018**, *9*, 1933. [CrossRef] [PubMed]
2. Dungey, H.S.; Dash, J.P.; Pont, D.; Clinton, P.W.; Watt, M.S.; Telfer, E.J. Phenotyping whole forests will help to track genetic performance. *Trends Plant Sci.* **2018**, *23*, 854–864. [CrossRef] [PubMed]
3. Pont, D.; Dungey, H.S.; Suontama, M.; Stovold, G.T. Spatial Models with Inter-Tree Competition from Airborne Laser Scanning Improve Estimates of Genetic Variance. *Front. Plant Sci.* **2020**, *11*, 596315. [CrossRef] [PubMed]
4. Bombrun, M.; Dash, J.P.; Pont, D.; Watt, M.S.; Pearse, G.D.; Dungey, H.S. Forest-scale phenotyping: Productivity characterisation through machine learning. *Front. Plant Sci.* **2020**, *11*, 99. [CrossRef]
5. Hartley, R.J.; Leonardo, E.M.; Massam, P.; Watt, M.S.; Estarija, H.J.; Wright, L.; Melia, N.; Pearse, G.D. An assessment of high-density UAV point clouds for the measurement of young forestry trials. *Remote Sens.* **2020**, *12*, 4039. [CrossRef]
6. Pearse, G.D.; Watt, M.S.; Dash, J.P.; Stone, C.; Caccamo, G. Comparison of models describing forest inventory attributes using standard and voxel-based lidar predictors across a range of pulse densities. *Int. J. Appl. Earth Obs. Geoinf.* **2019**, *78*, 341–351. [CrossRef]
7. Pont, D. Assessment of Individual Trees Using Aerial Laser Scanning in New Zealand Radiata Pine Forests. Ph.D. Thesis, University of Canterbury, Christchurch, New Zealand, 2016. Available online: https://hdl.handle.net/10092/12872 (accessed on 5 November 2021).
8. Watt, M.S.; Meredith, A.; Watt, P.; Gunn, A. The influence of LiDAR pulse density on the precision of inventory metrics in young unthinned Douglas-fir stands during initial and subsequent LiDAR acquisitions. *N. Z. J. For. Sci.* **2014**, *44*, 18. [CrossRef]
9. Windrim, L.; Bryson, M. Detection, Segmentation, and Model Fitting of Individual Tree Stems from Airborne Laser Scanning of Forests Using Deep Learning. *Remote Sens.* **2020**, *12*, 1469. [CrossRef]
10. Kellner, J.R.; Armston, J.; Birrer, M.; Cushman, K.; Duncanson, L.; Eck, C.; Falleger, C.; Imbach, B.; Král, K.; Krůček, M. New opportunities for forest remote sensing through ultra-high-density drone lidar. *Surv. Geophys.* **2019**, *40*, 959–977. [CrossRef]
11. Thies, M.; Pfeifer, N.; Winterhalder, D.; Gorte, B.G. Three-dimensional reconstruction of stems for assessment of taper, sweep and lean based on laser scanning of standing trees. *Scand. J. For. Res.* **2004**, *19*, 571–581. [CrossRef]
12. Hopkinson, C.; Chasmer, L.; Young-Pow, C.; Treitz, P. Assessing forest metrics with a ground-based scanning lidar. *Can. J. For. Res.* **2004**, *34*, 573–583. [CrossRef]
13. Lovell, J.; Jupp, D.L.; Culvenor, D.; Coops, N. Using airborne and ground-based ranging lidar to measure canopy structure in Australian forests. *Can. J. Remote Sens.* **2003**, *29*, 607–622. [CrossRef]
14. Watt, P.J.; Donoghue, D.N.M. Measuring forest structure with terrestrial laser scanning. *Int. J. Remote Sens.* **2005**, *26*, 1437–1446. [CrossRef]
15. Kankare, V.; Joensuu, M.; Vauhkonen, J.; Holopainen, M.; Tanhuanpää, T.; Vastaranta, M.; Hyyppä, J.; Hyyppä, H.; Alho, P.; Rikala, J.; et al. Estimation of the timber quality of scots pine with terrestrial laser scanning. *Forests* **2014**, *5*, 1879–1895. [CrossRef]
16. Abegg, M.; Kükenbrink, D.; Zell, J.; Schaepman, M.E.; Morsdorf, F. Terrestrial laser scanning for forest inventories-tree diameter distribution and scanner location impact on occlusion. *Forests* **2017**, *8*, 184. [CrossRef]
17. Mengesha, T.; Hawkins, M.; Tarleton, M.; Nieuwenhuis, M. Stem quality assessment using terrestrial laser scanning technology: A case study of ash trees with a range of defects in two stands in Ireland. *Scand. J. For. Res.* **2015**, *30*, 605–616. [CrossRef]
18. Liang, X.; Kankare, V.; Hyyppä, J.; Wang, Y.; Kukko, A.; Haggrén, H.; Yu, X.; Kaartinen, H.; Jaakkola, A.; Guan, F.; et al. Terrestrial laser scanning in forest inventories. *ISPRS J. Photogramm. Remote Sens.* **2016**, *115*, 63–77. [CrossRef]
19. Newnham, G.J.; Armston, J.D.; Calders, K.; Disney, M.I.; Lovell, J.L.; Schaaf, C.B.; Strahler, A.H.; Danson, F.M. Terrestrial laser scanning for plot-scale forest measurement. *Curr. For. Rep.* **2015**, *1*, 239–251. [CrossRef]
20. Raumonen, P.; Åkerblom, M.; Kaasalainen, M.; Casella, E.; Calders, K.; Murphy, S. Massive-scale tree modelling from TLS data. *ISPRS Ann. Photogramm. Remote Sens. Spat. Inf. Sci.* **2015**, *2*, 189–196. [CrossRef]
21. Liang, X.; Hyyppä, J.; Kaartinen, H.; Lehtomäki, M.; Pyörälä, J.; Pfeifer, N.; Holopainen, M.; Brolly, G.; Francesco, P.; Hackenberg, J.; et al. International benchmarking of terrestrial laser scanning approaches for forest inventories. *ISPRS J. Photogramm. Remote Sens.* **2018**, *144*, 137–179. [CrossRef]
22. Cabo, C.; Del Pozo, S.; Rodríguez-Gonzálvez, P.; Ordóñez, C.; González-Aguilera, D. Comparing terrestrial laser scanning (TLS) and wearable laser scanning (WLS) for individual tree modeling at plot level. *Remote Sens.* **2018**, *10*, 540. [CrossRef]
23. Holopainen, M.; Kankare, V.; Vastaranta, M.; Liang, X.; Lin, Y.; Vaaja, M.; Yu, X.; Hyyppä, J.; Hyyppä, H.; Kaartinen, H. Tree mapping using airborne, terrestrial and mobile laser scanning–A case study in a heterogeneous urban forest. *Urban For. Urban Green.* **2013**, *12*, 546–553. [CrossRef]

24. Bauwens, S.; Bartholomeus, H.; Calders, K.; Lejeune, P. Forest inventory with terrestrial LiDAR: A comparison of static and hand-held mobile laser scanning. *Forests* **2016**, *7*, 127. [CrossRef]
25. Ryding, J.; Williams, E.; Smith, M.J.; Eichhorn, M.P. Assessing handheld mobile laser scanners for forest surveys. *Remote Sens.* **2015**, *7*, 1095–1111. [CrossRef]
26. Hyyppä, E.; Yu, X.; Kaartinen, H.; Hakala, T.; Kukko, A.; Vastaranta, M.; Hyyppä, J. Comparison of backpack, handheld, under-canopy UAV, and above-canopy UAV laser scanning for field reference data collection in boreal forests. *Remote Sens.* **2020**, *12*, 3327. [CrossRef]
27. Shao, J.; Zhang, W.; Mellado, N.; Wang, N.; Jin, S.; Cai, S.; Luo, L.; Lejemble, T.; Yan, G. SLAM-aided forest plot mapping combining terrestrial and mobile laser scanning. *ISPRS J. Photogramm. Remote Sens.* **2020**, *163*, 214–230. [CrossRef]
28. Bienert, A.; Georgi, L.; Kunz, M.; Maas, H.G.; von Oheimb, G. Comparison and combination of mobile and terrestrial laser scanning for natural forest inventories. *Forests* **2018**, *8*, 395. [CrossRef]
29. Tang, J.; Chen, Y.; Kukko, A.; Kaartinen, H.; Jaakkola, A.; Khoramshahi, E.; Hakala, T.; Hyyppä, J.; Holopainen, M.; Hyyppä, H. SLAM-aided stem mapping for forest inventory with small-footprint mobile LiDAR. *Forests* **2015**, *6*, 4588–4606. [CrossRef]
30. Zhang, W.; Wan, P.; Wang, T.; Cai, S.; Chen, Y.; Jin, X.; Yan, G. A novel approach for the detection of standing tree stems from plot-level terrestrial laser scanning data. *Remote Sens.* **2019**, *11*, 211. [CrossRef]
31. Bu, G.; Wang, P. Adaptive circle-ellipse fitting method for estimating tree diameter based on single terrestrial laser scanning. *J. Appl. Remote Sens.* **2016**, *10*, 026040. [CrossRef]
32. Buck, A.L.B.; Lingnau, C.; Neto, S.P.; Machado, Á.M.L.; Martins-Neto, R.P. Stem modelling of eucalyptus by terrestrial laser scanning. *Floresta E Ambiente* **2019**, *26*, 1–10. [CrossRef]
33. Boudon, F.; Preuksakarn, C.; Ferraro, P.; Diener, J.; Nacry, P.; Nikinmaa, E.; Godin, C. Quantitative assessment of automatic reconstructions of branching systems obtained from laser scanning. *Ann. Bot.* **2014**, *114*, 853–862. [CrossRef]
34. Bruggisser, M.; Hollaus, M.; Otepka, J.; Pfeifer, N. Influence of ULS acquisition characteristics on tree stem parameter estimation. *ISPRS J. Photogramm. Remote Sens.* **2020**, *168*, 28–40. [CrossRef]
35. Torresan, C.; Carotenuto, F.; Chiavetta, U.; Miglietta, F.; Zaldei, A.; Gioli, B. Individual tree crown segmentation in two-layered dense mixed forests from uav lidar data. *Drones* **2020**, *4*, 10. [CrossRef]
36. Dash, J.P.; Watt, M.S.; Hartley, R.J.L. Testing UAV-Borne Riegl Mini VUX-1 Scanner for Phenotyping a Mature Genetics Trial. In *Technical Notes from the Growing Confidence in Forestry's Future Research Programme*; Scion: Rotorua, New Zealand, 2019; Volume TN-023. Available online: https://gcff.nz/publications/technical-notes/ (accessed on 1 May 2020).
37. Escandón, M.; Valledor, L.; Pascual, J.; Pinto, G.; Cañal, M.J.; Meijón, M. System-wide analysis of short-term response to high temperature in Pinus radiata. *J. Exp. Bot.* **2017**, *68*, 3629–3641. [CrossRef]
38. Yan, H.; Bi, H.; Li, R.; Eldridge, R.; Wu, Z.; Li, Y.; Simpson, J. Assessing climatic suitability of Pinus radiata (D. Don) for summer rainfall environment of southwest China. *For. Ecol. Manag.* **2006**, *234*, 199–208. [CrossRef]
39. Cabo, C.; Ordóñez, C.; López-Sánchez, C.A.; Armesto, J. Automatic dendrometry: Tree detection, tree height and diameter estimation using terrestrial laser scanning. *Int. J. Appl. Earth Obs. Geoinf.* **2018**, *69*, 164–174. [CrossRef]
40. Rais, A.; Poschenrieder, W.; Pretzsch, H.; van de Kuilen, J.-W.G. Influence of initial plant density on sawn timber properties for Douglas-fir (Pseudotsuga menziesii (Mirb.) Franco). *Ann. For. Sci.* **2014**, *71*, 617–626. [CrossRef]
41. Grace, J.; Pont, D.; Goulding, C.; Rawley, B. Modelling branch development for forest management. *N. Z. J. For. Sci.* **1999**, *29*, 391–408.
42. Dassot, M.; Colin, A.; Santenoise, P.; Fournier, M.; Constant, T. Terrestrial laser scanning for measuring the solid wood volume, including branches, of adult standing trees in the forest environment. *Comput. Electron. Agric.* **2012**, *89*, 86–93. [CrossRef]
43. Du, S.; Lindenbergh, R.; Ledoux, H.; Stoter, J.; Nan, L. AdTree: Accurate, detailed, and automatic modelling of laser-scanned trees. *Remote Sens.* **2019**, *11*, 2074. [CrossRef]
44. Fang, R.; Strimbu, B.M. Comparison of mature Douglas-firs' crown structures developed with two quantitative structural models using TLS point clouds for neighboring trees in a natural regime stand. *Remote Sens.* **2019**, *11*, 1661. [CrossRef]
45. Pyörälä, J.; Liang, X.; Vastaranta, M.; Saarinen, N.; Kankare, V.; Wang, Y.; Holopainen, M.; Hyyppä, J. Quantitative assessment of Scots pine (Pinus sylvestris L.) whorl structure in a forest environment using terrestrial laser scanning. *IEEE J. Sel. Top. Appl. Earth Obs. Remote Sens.* **2018**, *11*, 3598–3607. [CrossRef]
46. Harikumar, A.; Bovolo, F.; Xinlian, L. An effective approach to 3D stem modeling and branch-knot localization in multiscan TLS data. In Proceedings of the International Geoscience and Remote Sensing Symposium (IGARSS), Yokohama, Japan, 28 July–2 August 2019; pp. 6075–6078.
47. Stängle, S.M.; Brüchert, F.; Kretschmer, U.; Spiecker, H.; Sauter, U.H. Clear wood content in standing trees predicted from branch scar measurements with terrestrial LiDAR and verified with X-ray computed tomography. *Can. J. For. Res.* **2014**, *44*, 145–153. [CrossRef]
48. CNI Regional YTGEN User Group. *PlotSafe: Overlapping Feature Cruising. Forest Inventory Procedures*; CNI Regional YTGEN User Group: Rotorua, New Zealand, 2007.
49. Wallace, L.O.; Lucieer, A.; Watson, C.S. Assessing the feasibility of UAV-based lidar for high resolution forest change detection. In Proceedings of the International Archives of the Photogrammetry, Remote Sensing and Spatial Information Sciences-ISPRS Archives, Melbourne, Australia, 25 August–1 September 2012; pp. 499–504.

50. Hackenberg, J.; Calders, K.; Demol, M.; Raumonen, P.; Piboule, A.; Disney, M. SimpleForest-a comprehensive tool for 3d reconstruction of trees from forest plot point clouds. *BioRxiv* **2021**. [CrossRef]
51. Dijkstra, E.W. A note on two problems in connexion with graphs. *Numer. Math.* **1959**, *1*, 269–271. [CrossRef]
52. R Core Team. *R: A Language and Environment for Statistical Computing*; R Foundation for Statistical Computing: Vienna, Austria, 2020.
53. De Conto, T.; Olofsson, K.; Görgens, E.B.; Rodriguez, L.C.E.; Almeida, G. Performance of stem denoising and stem modelling algorithms on single tree point clouds from terrestrial laser scanning. *Comput. Electron. Agric.* **2017**, *143*, 165–176. [CrossRef]
54. Roussel, J.-R.; Auty, D.; De Boissieu, F.; Meador, A. *lidR: Airborne LiDAR Data Manipulation and Visualization for Forestry Applications, R Package Version*; R Foundation for Statistical Computing: Vienna, Austria, 2018; Volume 1.
55. Kuhn, M. Building predictive models in R using the caret package. *J. Stat. Softw.* **2008**, *28*, 1–26. [CrossRef]
56. Zhong, L.; Cheng, L.; Xu, H.; Wu, Y.; Chen, Y.; Li, M. Segmentation of individual trees from TLS and MLS data. *IEEE J. Sel. Top. Appl. Earth Obs. Remote Sens.* **2017**, *10*, 774–787. [CrossRef]
57. Bienert, A.; Georgi, L.; Kunz, M.; von Oheimb, G.; Maas, H.-G. Automatic extraction and measurement of individual trees from mobile laser scanning point clouds of forests. *Ann. Bot.* **2021**, *128*, 787–804. [CrossRef]
58. Giannetti, F.; Puletti, N.; Quatrini, V.; Travaglini, D.; Bottalico, F.; Corona, P.; Chirici, G. Integrating terrestrial and airborne laser scanning for the assessment of single-tree attributes in Mediterranean forest stands. *Eur. J. Remote Sens.* **2018**, *51*, 795–807. [CrossRef]
59. Calders, K.; Newnham, G.; Burt, A.; Murphy, S.; Raumonen, P.; Herold, M.; Culvenor, D.; Avitabile, V.; Disney, M.; Armston, J.; et al. Nondestructive estimates of above-ground biomass using terrestrial laser scanning. *Methods Ecol. Evol.* **2015**, *6*, 198–208. [CrossRef]
60. Chen, S.; Feng, Z.; Chen, P.; Khan, T.U.; Lian, Y. Nondestructive estimation of the above-ground biomass of multiple tree species in boreal forests of china using terrestrial laser scanning. *Forests* **2019**, *10*, 936. [CrossRef]
61. Čerňava, J.; Tuček, J.; Koreň, M.; Mokroš, M. Estimation of diameter at breast height from mobile laser scanning data collected under a heavy forest canopy. *J. For. Sci.* **2017**, *63*, 433–441. [CrossRef]
62. Brolly, G.; Király, G. Algorithms for stem mapping by means of terrestrial laser scanning. *Acta Silv. Et Lignaria Hung.* **2009**, *5*, 119–130.
63. Fleck, S.; Mölder, I.; Jacob, M.; Gebauer, T.; Jungkunst, H.F.; Leuschner, C. Comparison of conventional eight-point crown projections with LIDAR-based virtual crown projections in a temperate old-growth forest. *Ann. For. Sci.* **2011**, *68*, 1173–1185. [CrossRef]
64. Huang, H.; Li, Z.; Gong, P.; Cheng, X.; Clinton, N.; Cao, C.; Ni, W.; Wang, L. Automated methods for measuring DBH and tree heights with a commercial scanning lidar. *Photogramm. Eng. Remote Sens.* **2011**, *77*, 219–227. [CrossRef]
65. Liang, X.; Hyyppä, J. Automatic stem mapping by merging several terrestrial laser scans at the feature and decision levels. *Sensors* **2013**, *13*, 1614–1634. [CrossRef]
66. Maas, H.G.; Bienert, A.; Scheller, S.; Keane, E. Automatic forest inventory parameter determination from terrestrial laser scanner data. *Int. J. Remote Sens.* **2008**, *29*, 1579–1593. [CrossRef]
67. Moskal, L.M.; Zheng, G. Retrieving forest inventory variables with terrestrial laser scanning (TLS) in urban heterogeneous forest. *Remote Sens.* **2012**, *4*, 1–20. [CrossRef]
68. Puliti, S.; Dash, J.P.; Watt, M.S.; Breidenbach, J.; Pearse, G.D. A comparison of UAV laser scanning, photogrammetry and airborne laser scanning for precision inventory of small-forest properties. *Forestry* **2020**, *93*, 150–162. [CrossRef]
69. Sankey, T.; Donager, J.; McVay, J.; Sankey, J.B. UAV lidar and hyperspectral fusion for forest monitoring in the southwestern USA. *Remote Sens. Environ.* **2017**, *195*, 30–43. [CrossRef]
70. Corte, A.P.D.; Rex, F.E.; de Almeida, D.R.A.; Sanquetta, C.R.; Silva, C.A.; Moura, M.M.; Wilkinson, B.; Zambrano, A.M.A.; da Cunha Neto, E.M.; Veras, H.F.P.; et al. Measuring individual tree diameter and height using gatoreye high-density UAV-lidar in an integrated crop-livestock-forest system. *Remote Sens.* **2020**, *12*, 863. [CrossRef]
71. Jaakkola, A.; Hyyppä, J.; Yu, X.; Kukko, A.; Kaartinen, H.; Liang, X.; Hyyppä, H.; Wang, Y. Autonomous collection of forest field reference—The outlook and a first step with UAV laser scanning. *Remote Sens.* **2017**, *9*, 785. [CrossRef]
72. Camarretta, N.; Harrison, P.A.; Lucieer, A.; Potts, B.M.; Davidson, N.; Hunt, M. From drones to phenotype: Using UAV-LiDAR to detect species and provenance variation in tree productivity and structure. *Remote Sens.* **2020**, *12*, 3184. [CrossRef]
73. Liang, X.; Wang, Y.; Pyörälä, J.; Lehtomäki, M.; Yu, X.; Kaartinen, H.; Kukko, A.; Honkavaara, E.; Issaoui, A.E.I.; Nevalainen, O.; et al. Forest in situ observations using unmanned aerial vehicle as an alternative of terrestrial measurements. *For. Ecosyst.* **2019**, *6*, 20. [CrossRef]
74. Ayrey, E.; Fraver, S.; Kershaw, J.A., Jr.; Kenefic, L.S.; Hayes, D.; Weiskittel, A.R.; Roth, B.E. Layer stacking: A novel algorithm for individual forest tree segmentation from LiDAR point clouds. *Can. J. Remote Sens.* **2017**, *43*, 16–27. [CrossRef]
75. Wang, Y.; Lehtomäki, M.; Liang, X.; Pyörälä, J.; Kukko, A.; Jaakkola, A.; Liu, J.; Feng, Z.; Chen, R.; Hyyppä, J. Is field-measured tree height as reliable as believed–A comparison study of tree height estimates from field measurement, airborne laser scanning and terrestrial laser scanning in a boreal forest. *ISPRS J. Photogramm. Remote Sens.* **2019**, *147*, 132–145. [CrossRef]
76. Larjavaara, M.; Muller-Landau, H.C. Measuring tree height: A quantitative comparison of two common field methods in a moist tropical forest. *Methods Ecol. Evol.* **2013**, *4*, 793–801. [CrossRef]

77. Saarinen, N.; Kankare, V.; Vastaranta, M.; Luoma, V.; Pyörälä, J.; Tanhuanpää, T.; Liang, X.; Kaartinen, H.; Kukko, A.; Jaakkola, A. Feasibility of Terrestrial laser scanning for collecting stem volume information from single trees. *ISPRS J. Photogramm. Remote Sens.* **2017**, *123*, 140–158. [CrossRef]
78. Murphy, G. Determining stand value and log product yields using terrestrial lidar and optimal bucking: A case study. *J. For.* **2008**, *106*, 317–324.
79. Brede, B.; Calders, K.; Lau, A.; Raumonen, P.; Bartholomeus, H.M.; Herold, M.; Kooistra, L. Non-destructive tree volume estimation through quantitative structure modelling: Comparing UAV laser scanning with terrestrial LIDAR. *Remote Sens. Environ.* **2019**, *233*, 111355. [CrossRef]
80. Wang, D.; Hollaus, M.; Puttonen, E.; Pfeifer, N. Automatic and self-adaptive stem reconstruction in landslide-affected forests. *Remote Sens.* **2016**, *8*, 974. [CrossRef]